Sustainable Food Technology

ROYAL SOCIETY OF CHEMISTRY

PAPER

View Article Online
View Journal | View Issue

Check for updates

Cite this: *Sustainable Food Technol.*, 2026, 4, 823

# Assessing the antibacterial, antifungal, and antiaflatoxigenic activity of a developed nanoformulation based on a combination of *Syzygium aromaticum* leaf and bud essential oils

Tanya Singh Raghuvanshi,[a] Vishal Gupta[b] and Bhanu Prakash *[a]

Received 30th July 2025
Accepted 31st October 2025

DOI: 10.1039/d5fb00440c

rsc.li/susfoodtech

The increase in mycotoxin contamination and antimicrobial resistance draws attention towards the development of natural broad-spectrum antimicrobial compounds. Recent studies have highlighted the use of nanoencapsulated essential oils as a promising natural antimicrobial agent and a safer alternative to the synthetic ones. This study investigates the inherent antibacterial, antifungal, and antiaflatoxigenic potential of a nanoencapsulated formulation developed from a combination of essential oils extracted from *Syzygium aromaticum* leaves and buds. The GC-MS analysis of this combination (SACEO) confirmed the presence of meta-eugenol as the major bioactive component. The SACEO demonstrated synergistic activity, which was further stabilized *via* nanoencapsulation (Ne-SACEO) and was found to have steady dispersion, a favorable zeta potential, and a homogeneous size through physicochemical characterization. Ne-SACEO demonstrated significant antioxidative potential, lower MAIC and MIC values than SACEO for aflatoxin $B_1$ (0.15; 0.2 μL $mL^{-1}$), *Aspergillus flavus* (0.35; 0.40 μL $mL^{-1}$), *B. cereus* (50; 72.66 ppm), *E. coli* (56.66; 67.33 ppm), *S. enterica* (54.66; 64.66 ppm), and *S. flexneri* (64; 76 ppm) respectively, indicating increased bioefficacy. According to mechanistic investigations, Ne-SACEO impaired the integrity of fungal and bacterial cells, leading to cell death. The combined antimicrobial and anti-aflatoxigenic activity of Ne-SACEO, supported by sustained release, improved solubility, and membrane permeability, highlights its potential as a green multifunctional biopreservative agent in food safety and sustainability.

Open Access Article. Published on 01 2025. Downloaded on 21/06/2026 23:23:45.
This article is licensed under a Creative Commons Attribution-NonCommercial 3.0 Unported Licence.

**Sustainability spotlight**

The increase in mycotoxin contamination and antimicrobial resistance draws attention towards the development of natural and broad-spectrum antimicrobial compounds. The study reports the antimicrobial efficacy and probable mechanism of a developed synergistic nanoformulation based on the combination of clove leaf and bud essential oils (EOs), and recommends its application as a novel sustainable alternative to synthetic chemicals.

## 1. Introduction

Mycotoxin contamination and foodborne infections continue to be major global public health concerns, particularly in low- and middle-income countries where food storage and hygiene standards are frequently inadequate. Foodborne outbreaks are largely caused by bacterial pathogens, including *Salmonella enterica*, *Clostridium botulinum*, *Escherichia coli*, *Bacillus cereus, Listeria monocytogenes*, *etc.* These pathogens cause gastrointestinal disorders that can result in serious morbidity and sometimes be fatal.[1,2] The bacterial foodborne illnesses are related to the high-risk sources, including raw vegetables, undercooked meat, infected cereals, and unpasteurized dairy. The infection of *E. coli* can be linked to hemorrhagic colitis and hemolytic uremic syndrome (HUS), which can occasionally result in renal failure.[3] *B. cereus* can cause emesis and diarrhoeal food poisoning, proliferating under unfavorable storage conditions, and is heat resistant.[4] *S. enterica* and *S. flexneri* are responsible for typhoid fever and shigellosis, respectively, under unhygienic conditions.[5,6]

Fungal contamination is one of the most common reasons for loss of important commodities and a cause of imbalance in gut health. Among the known fungal secondary metabolites, Aflatoxin $B_1$ ($AFB_1$), a powerful carcinogen (the International Agency for Research on Cancer (IARC) classifies it as a Group I carcinogen), compromises the health of both humans and animals. These biological risks drastically lower the safety and

[a]*Department of Botany, Institute of Science, Banaras Hindu University, Varanasi, 221005, India*

[b]*Department of Botany, Mahatma Gandhi Post Graduate College, Gorakhpur, 273001 Uttar Pradesh, India. E-mail: bprakash@bhu.ac.in; Tel: +91-9794113055*

© 2026 The Author(s). Published by the Royal Society of Chemistry

Open Access Article. Published on 01 2025. Downloaded on 21/06/2026 23:23:45.
This article is licensed under a Creative Commons Attribution-NonCommercial 3.0 Unported Licence.

quality of food and cause huge financial losses as a result of crop rejection, deterioration, and export prohibitions.[7] Among all known $AFB_1$-producing fungi, *A. flavus* is highly prevalent in food commodities, including cereals, nuts, oilseeds, and dairy substitutes, especially in warm humid climates. Exposure to $AFB_1$ has been associated with growth retardation, immunosuppression, liver cancer, and in severe cases, acute poisoning. Aflatoxin contamination risks have increased recently, particularly in tropical and subtropical regions, due to factors such as climate change, growing international trade, and inadequate post-harvest handling. Therefore, one of the top priorities in the discipline of food safety is to identify sustainable and efficient ways to regulate the proliferation of *A. flavus* and its toxins.[8,9]

Globalized food chains and the emergence of antibiotic-resistant bacteria have complicated control of these food-borne illnesses. The range of available treatments is restricted by the advent of organisms that are multidrug resistant. Such concerns draw attention to the necessity of safe, plant-based antimicrobials to improve food safety and control the growing threat of foodborne pathogens.[10]

Hence, researchers are investigating natural alternatives in response to the health risks associated with synthetic food preservatives and the rise in antibiotic resistance. Aromatic plants, which are often abundant in volatile substances including phenols, aldehydes, terpenes, and alcohols, are capable of damaging microbial cells and are one of the alternatives. Because of their antibacterial, antifungal, antioxidant, and insecticidal qualities, essential oils (EOs) extracted from these plants are gaining interest as promising bioactive agents.[11]

The medicinal plant *S. aromaticum*, frequently referred to as clove, is utilized extensively for its antioxidant and antibacterial qualities, which are mostly brought about by the presence of bioactive compounds.[12] Clove's leaves and flower buds (two slightly different essential oils) have been widely studied individually; combining these two oils was anticipated to have the potential to provide additive or synergistic antimicrobial actions because of their complementary chemical compositions. The developed formulation could have better bioactivity and can be a novel source of antimicrobial agent. Furthermore, encapsulation of this combination in a chitosan-cinnamic acid nanomatrix can help stabilize and protect the volatile compound, increasing the bioefficacy.

This study aims to develop a chitosan-cinnamic acid nanomatrix encapsulated bioactive formulation by combining essential oils from clove leaves and buds. The chemical profile of the developed formulation was assessed *via* GC-MS analysis. Furthermore, we investigated its antifungal, antiaflatoxigenic, and antibacterial potential. In addition, effects of nano-encapsulation on the formulation's antimicrobial properties and the mechanism of action were demonstrated using biochemical and *in silico* approaches. The research specifically targets the antimicrobial activity and underlying functional principle of *in vitro* inhibition of foodborne bacterial pathogens (*E. coli*, *S. Typhi*, *B. cereus*, and *S. flexneri*), the toxigenic fungus *A. flavus* (*AfAh0723*), and $AFB_1$ production.

# 2. Materials and methods

## 2.1. Materials and reagents

All the chemicals used in the present study were procured from Sisco Research Laboratories Pvt. Ltd (Mumbai, India), Hi-media (Maharashtra, India), and Sigma-Aldrich (St. Louis, MO, United States). The low molecular weight deacetylated chitosan was purchased from Sigma-Aldrich. The major equipment used in the study was a hydro-distillation unit (Merck Specialities Pvt. Ltd, Mumbai, India), gas chromatograph-mass spectrometer (PerkinElmer, Turbomass Gold, USA), atomic absorption spectrophotometer (PerkinElmer, AAnalyst 800, USA), spectrophotometer from Shimadzu (UV 1800), and cooling centrifuge (CPR-24 plus).[13,14]

## 2.2. Microbial strains and culture conditions

The research includes mold species, *Aspergillus flavus* strain (AfAh0723), which was previously isolated in our laboratory from *Arachis hypogaea* seeds, and the active culture was maintained on Potato Dextrose Agar (PDA), pH 5.4–6.0 at 27 ± 2 °C. The spore suspension was maintained in autoclaved Milli-Q water at +4 °C, which was used as inoculum in the study.

The study included four food-borne bacterial isolates: *Shigella flexneri* (MTCC no. 1457), *Salmonella enterica* ser. *typhi* (MTCC no. 733), *Bacillus cereus* (MTCC no. 1272), and *Escherichia coli* (MTCC no. 77). The source of these bacterial isolates was the Microbial Type Culture Collection and Gene Bank, India. Pure bacterial slants were kept in a refrigerator on nutrient agar (NA), whereas all bacterial cultures were maintained on nutrient broth (NB) at 37 ± 2 °C, which was further used as inoculum in the study.

## 2.3. Extraction, combination, and chemical profiling of SACEO by GC-MS

The leaves of the *S. aromaticum* plant were collected from the Botanical Garden, Department of Botany, Banaras Hindu University, Varanasi, India. The bud of *S. aromaticum* was purchased separately from a local shop near B.H.U., Varanasi.

The essential oils from leaves and buds were extracted separately using the hydrodistillation method by adding fine pieces of fresh leaves (200 g) and crushed buds (50 g), mixing with double-distilled water, and heating at 90 °C for 4 h using the Clevenger apparatus.[15,16] After extraction, the remaining moisture from both oils was removed using anhydrous sodium sulfate, and the pure oils were stored at 4 °C for future use.[17] Both of these oils were separately tested against bacteria as well as fungi, and further combined in different ratios (leaf: buds-1 : 1, 1 : 2, 2 : 1, 1 : 3, and 3 : 1) to analyze the potential of their combination.[18] The fourth combination, *i.e.*, 1 : 3, was found to be the most potent and thus further subjected to chemical characterization using GC-MS using an Elite-5 capillary column. The separation was carried out with a 30 m Elite-5 capillary column, and a 1 μL injection volume (1 : 50 diluted in acetone). The chemical profile of the SACEO was determined by comparing its mass spectral pattern with the mass spectral libraries of the Wiley, NIST, and NBS.[13,14]


© 2026 The Author(s). Published by the Royal Society of Chemistry

Open Access Article. Published on 01 2025. Downloaded on 21/06/2026 23:23:45. This article is licensed under a Creative Commons Attribution-NonCommercial 3.0 Unported Licence.

### 2.4. Preparation of the chitosan nanogel and encapsulation of SACEO

For the preparation of the nanogel, 0.5 g of chitosan was dissolved in 100 mL of 1% aqueous acetic acid solution and kept on a magnetic stirrer for 18 hours at 400 rpm. After 18 hours, the solution was diluted with 85 mL of methanol, and the pH was adjusted to 3.5–4.0. The solution was sonicated at 50 Hz for 5 min to reduce and even out the particle size. A separate solution was prepared by dissolving 317.5 mg of cinnamic acid in 669 μL of EDC. This solution was added to 75 mL of the sonicated chitosan solution dropwise and then kept on a magnetic stirrer for 24 hours at 250 rpm to ensure the homogenization of the resulting solution. The pH of the final solution was adjusted between 8.5–9.0, and then centrifuged at 9000 rpm for 15 min to pellet down the synthesized nanogel. The pellet was washed twice with double distilled water and ethanol. This pure nanogel was vacuum lyophilized for 24 hours, and the weight of the dry nanogel was recorded.[19]

Furthermore, 100 mg of the dry gel was resuspended in 10 mL of 0.1% aqueous acetic acid solution on a magnetic stirrer at 250 rpm, and the pH was adjusted to 3.5–4.0. This sample was filtered using Whatman filter paper to have even-sized particles in the final solution. Subsequently, multiple quantities of SACEO were added to the synthesized nanogel to achieve different ratios of the chitosan nanogel to SACEO (1 : 0.25, 1 : 0.5, 1 : 0.75, and 1 : 1) and subjected to sonication at 50 Hz for 20 minutes using a probe-type sonicator.

### 2.5. Characterization of Ne-SACEO

The incorporation of SACEO within the chitosan nanoparticles (CSNPs) was validated by Dynamic Light Scattering (DLS), Fourier Transform Infrared Spectroscopy (FTIR), and X-ray Diffraction (XRD).

**2.5.1. Dynamic light scattering (DLS).** The average particle size and zeta potential of the synthesized chitosan nanogel and nanoencapsulated combination (Ne-SACEO) were measured by dynamic light scattering (DLS) (Zeta sizer, Malvern Instrument, UK). The measurements assessed the dispersion uniformity, colloidal stability, and surface charge characteristics of the nanoparticles, which are essential indications of nanogel efficacy in biological and food systems.[20]

**2.5.2. ATR-FTIR analysis.** ATR-FTIR spectra of chitosan, CSNPs, SACEO, and Ne-SACEO were recorded using an attenuated total reflection-fourier transform infrared spectrometer using chitosan powder and liquid samples of CSNPs, SACEO, and Ne-SACEO in the wavenumber range of 400–4000 $cm^{-1}$.[21–23]

**2.5.3. X-ray diffraction (XRD) analysis.** To ascertain whether the substance was crystalline or amorphous, the encapsulating products, such as low molecular weight chitosan, chitosan-cinnamic acid nanogel, and Ne-CIM, were subjected to high-resolution analysis *via* X-ray diffractometry (Bruker D8 Advance) across the $2\theta$ spectrum of 10–80°, employing a step size of 0.02° $min^{-1}$ and a scan speed of 5° $min^{-1}$.[24]

**2.5.4. Encapsulation efficiency and loading capacity.** EE and LC were estimated using the Onyebuchi *et al.*, 2019[25] technique. Briefly, 5 mL of aqueous hydrochloric acid (2 M) was mixed with 10 mg of Ne-SACEO and allowed to stand at 95 °C for 30 minutes. After the sample cooled down, 1 mL of methanol was added, and it was centrifuged for 5 minutes at 3000 rpm. The blank sample (CSNPs) was made in a similar manner. The absorbance maxima (at 281 nm and standard curve $R^2 = 0.998$) of SACEO, determined using a UV-vis spectrophotometer, were used to measure the amount of SACEO loaded into the CSNPs. The following formulas were used to determine the percent % EE and % LC:

$$\%\ \mathrm{EE} = \frac{\text{mass of loaded SACEO}}{\text{mass of initial SACEO}} \times 100$$

$$\%\ \mathrm{LC} = \frac{\text{total amount of loaded SACEO}}{\text{weight of freeze dried sample}} \times 100$$

The *in vitro* release of CLEO from the chitosan-cinnamic acid-based nanomatrix was measured using the method of Hosseini *et al.*, 2013[26] with minor changes. 0.5 mL of the loaded sample was taken in a microcentrifuge tube containing 5 mL of 40% alcoholic phosphate-buffered saline and stored at room temperature. At specific intervals, the sample was centrifuged for 6 minutes at 8800 rpm. The supernatant was separated, and pellet was redissolved in same quantity of fresh buffer. A UV-vis spectrophotometer was used to quantify the *in vitro* release of CLEO from the nanomatrix at regular time intervals at 270 nm.[27] The cumulative release was calculated as follows:

$$\%\ \text{cumulative release} = \frac{\text{cumulative amount of SACEO released at specific time}}{\text{amount of total SACEO}} \times 100$$

### 2.6. Free radical scavenging activity of Ne-SACEO

**2.6.1. DPPH.** 2,2-Diphenyl-1-picrylhydrazyl (DPPH), a relatively stable chemical radical, has been used extensively to assess the antioxidant activity of both the complex combinations and individual molecules. The basis of this assay lies on the fact that, in the presence of an antioxidant which donates hydrogen, free radicals present in an alcoholic DPPH solution decreases. In accordance with the protocol, the 2, 2-diphenyl-1-picrylhydrazyl (DPPH) radical assay was used to evaluate the capacity of Ne-SACEO to scavenge free radicals. After adding a 0.004% methanolic DPPH solution to different Ne-SACEO concentrations (0.005–0.035 μL $mL^{-1}$), the mixtures were allowed to stand at room temperature (27 ± 2 °C) in the dark for 30 minutes. The absorbance of the reaction mixtures was then

Open Access Article. Published on 01 2025. Downloaded on 21/06/2026 23:23:45. This article is licensed under a Creative Commons Attribution-NonCommercial 3.0 Unported Licence.

measured at 517 nm in comparison to the blank sample, which was a methanolic solution of DPPH without adding Ne-SACEO.[28] The mentioned formula was used to obtain the percentage inhibition of DPPH free radicals, and the graph of the percentage inhibition of DPPH against concentration was used to determine the $IC_{50}$ (concentration of Ne-SACEO at which 50% neutralization of DPPH radicals occurs).

$$\%\ \text{Inhibition} = (A_{\text{blank}} - A_{\text{sample}})/A_{\text{blank}}$$

Here,$A_{\text{Blank}}$ = absorbance of control (methanolic solution of DPPH) and $A_{\text{Sample}}$ = absorbance of samples with different doses of Ne-SACEO.

**2.6.2. ABTS.** The ABTS radical cation reagent was made by mixing 2.45 mM potassium persulfate with 7 mM ABTS solution. The reagent was stored at room temperature and in the dark. Different concentrations of essential oil were added to 2 mL of ABTS solution. The mixture was then vigorously shaken and allowed to stand at room temperature for 30 minutes in the dark. A PerkinElmer spectrophotometer was used to measure the solution's absorbance, which came out to be 734 nm. As a blank solution, methanol was employed without adding any essential oil to it.[29] The equation mentioned previously to calculate the percentage inhibition of DPPH free radical was used again to determine the scavenging capacity.

### 2.7. Antifungal activity of Ne-SACEO against food-borne *A. flavus* and its anti-aflatoxigenic potential

The *in vitro* antifungal activity of the EO against *A. flavus* was evaluated by the method reported in Prakash *et al.*, 2011.[30] 0.5% (v/v) Tween 20 was used to dissolve the required quantity of SALEO (0.1–0.7), SABEO (0.05–0.45), SACEO (0.05–0.40) and Ne-SACEO (0.05–0.35) in SMKY media, respectively, resulting in varying concentrations. In parallel to the treatment set, two control sets were maintained to monitor the growth under ideal conditions. Each treatment, including controls, was then added with 50 μL of the spore suspension (*A. flavus* strain) and incubated at 27 ± 2 °C. The minimum inhibitory concentration (MIC) was determined by measuring the lowest oil concentration at which no fungal growth was observed on the seventh day of incubation.[31,32] To determine the AFB1 inhibitory effect, the growth medium containing AFB1 secreted by *A. flavus* was filtered and purified using chloroform extraction.[33] The extracted toxin was subjected to chromatographic separation using a TLC plate. The fluorescent spot on the plate, comparable to the aflatoxin B1 standard, was collected and dissolved in methanol. The sample was centrifuged, and the optical density of the supernatant was recorded. Additionally, the formula mentioned was used to calculate the results in terms of the minimum aflatoxin B1 inhibitory concentration (MAIC):

$$AFB_1\ \text{content}\ (\mu g\ mL^{-1}) = (D \times M)/(E \times L) \times 1000$$

Here, $D$ = absorbance, $M$ = $AFB_1$ molecular weight (312), $E$ is the extinction coefficient (21 800), and $L$ = 1 cm.

### 2.8. Antifungal mechanism of action

**2.8.1. Effect of Ne-SACEO on ergosterol content in the plasma membrane of *A. flavus*.** The amount of ergosterol in *A. flavus* exposed to varying concentrations of Ne-SACEO (1/4 MIC, 1/2 MIC, and MIC) has been evaluated. After adding a 25% alcoholic KOH solution to 1 g of four-day-old mycelia that had been treated with various Ne-SACEO dosages (0.05–0.35) and along with the control set, they were vortexed for two minutes. Additionally, the solution was incubated for four hours at 85 °C in a water bath. The solution was then vortexed for two minutes after two millilitres of sterile distilled water and five millilitres of *n*-heptane were added. After two hours of stratification of two distinct layers, the upper transparent *n*-heptane layer was collected and scanned between 230–300 nm.[34] The ergosterol content has been quantified using the following formula:

$$\text{Ergosterol}\ (\%) = (A_{282/290} - A_{230/518})/W$$

Here,*A*: absorbance; 290 and 518 = extinction coefficient of ergosterol and dehydroergosterol, respectively; *W*: mycelial weight.

$$\%\ \text{Inhibition} = (E_{\text{control}} - E_{\text{treatment}})/E_{\text{control}} \times 100$$

Here,$E_{\text{control}}$: ergosterol content of control mycelia; $E_{\text{treatment}}$: ergosterol content of treated mycelia.

**2.8.2. Effect on cellular cation leakage.** *A. flavus* mycelia that had been cultured in liquid media (SMKY) for five days were harvested and suspended in 20 milliliters of 0.85% saline solution. This process was followed by fumigation with several concentrations of SACEO (ops). The solution containing the mycelial material was filtered after 12 hours and collected in a 50 mL beaker. Membrane cations (K+ and Mg++) were then measured in the filtrate using atomic absorption spectrometry (AAS).[35]

**2.8.3. Effect on mitochondrial membrane potential (MMP).** The technique mentioned in Tian *et al.* (2012)[36] was used to evaluate MMP. After dissolving *A. flavus* spores in 0.5% Tween 20, the non-treated sample (control) was treated with varying concentrations of Ne-SACEO (0.05–0.35 μL $mL^{-1}$) for 12 hours. The samples were incubated for five minutes and then centrifuged at 5000 rpm. The pellets were then dissolved in PBS containing 100 ng $mL^{-1}$ of Rhodamine 123 (Rh123) dye. Following a 15 minute incubation period in the dark, the samples were centrifuged once more at 5000 rpm for 5 minutes, and the intensity of Rh123 in the pellets was measured using a fluorescence spectrophotometer at 488 nm excitation and 525 nm emission wavelengths.[37]

**2.8.4. Determination of release of 260-nm and 280-nm absorbing materials.** Furthermore, for the determination of leakage of 260 and 280 (nucleic acid/protein) absorbing materials, five-day-old mycelia were thoroughly washed and transferred to 20 mL of PBS solution, respectively. It was exposed to the desired concentration of Ne-SACEO for 12 h at 25 ± 2 °C. For the leakage of 260 and 280 absorbing materials, the samples were centrifuged at 13 000 rpm for 15 minutes and the

 © 2026 The Author(s). Published by the Royal Society of Chemistry

Open Access Article. Published on 01 2025. Downloaded on 21/06/2026 23:23:45. This article is licensed under a Creative Commons Attribution-NonCommercial 3.0 Unported Licence.

absorbance of the supernatant was recorded at 260 and 280 nm using a UV-visible spectrophotometer.[38]

### 2.9. Anti-bacterial efficacy

**2.9.1. Preparation of bacterial inoculum.** In the current investigation, a nutrient agar medium plate was streaked and cultivated with *S. flexneri* (MTCC no. 1457), *S. enterica* ser. *typhi* (MTCC no. 733), *B. cereus* (MTCC no. 1272), and *E. coli* (MTCC no. 77). For each streaked plate, a single colony of all the bacteria was isolated and placed in a 200 mL nutrient broth (NB). It was incubated for 12 hours at 37 °C in an incubator shaker. Cells were collected by centrifugation (4000×*g*, 10 min, 4 °C) following incubation, and they were then washed twice. The harvested cells were then resuspended in 0.85% sterile saline solution and used in further experiments.

**2.9.2. MTT assay to determine the MIC of EOs.** To find the MIC of the SALEO, SABEO, SACEO, and Ne-SACEO, a 96-well disposable sterile microtiter plate was used in an MTT colorimetric test. Using DMSO as an emulsifier, stock solutions of each EO (10 μL $mL^{-1}$) were produced. To generate EO concentrations ranging from 0.02 to 0.12 μL $mL^{-1}$, diluted EO solutions were made from stock solutions using the NB broth medium as the solvent. 100 μL of each dilution was subsequently added in their respective wells. Each EO concentration was increased by 0.02 mg $mL^{-1}$ between two successive wells. After that, 100 μL of the 105 CFU per mL bacterial suspension was added to the plates, and an autoclavable sterile sealer mat was placed over them to operate as an efficient barrier and stop the volatile substances from affecting the nearby wells.[39] A similar set of experiments was repeated with neomycin sulfate as the standard antibacterial agent at the same concentration. Furthermore,10 μL of MTT reconstituted in PBS at 5 mg $mL^{-1}$ was applied to each well and incubated for 4 hours at 37 °C following a 24-hour incubation period. Dehydrogenases in living cells convert the yellow tetrazolium salt MTT into a purple formazan. Accordingly, the number of living cells directly correlates with the amount of formazan generated, and the minimum inhibitory concentration (MIC) is visible on the plates. In this manner, the lowest concentration at which no purple color was observed was used to calculate the MIC values.[40] The experiment was conducted in triplicate for each oil.

### 2.10. Antibacterial mechanism of action of Ne-SACEO

**2.10.1. Determination of membrane potential.** The rhodamine fluorescence method was used to monitor the membrane potential of the bacteria. After fresh bacterial cells were treated with varying doses of Ne-SACEO (1/4 MIC, 1/2 MIC, and MIC) in PBS solution, the suspension was incubated for 30 minutes in 2 μg $mL^{-1}$ Rhodamine 123 (Rh123) solution in order to visualise their metabolic activity. The cells were then washed with PBS and a fluorescence spectrophotometer was used to quantify the Rh123 fluorescence intensity of the control and samples treated with Ne-SACEO at 488 nm excitation and 525 nm emission wavelengths. The results were reported as mean fluorescence intensity (MFI).[41]

**2.10.2. Membrane fluidity analysis.** The analysis of membrane fluidity for each bacterial strain was done by growing all the bacteria in NB for 12 hours. The cell pellets were collected for each bacterial strain and calibrated to an $OD_{600}$ of 0.5. A 2 μM DPH solution was then added, and the mixture was incubated for 45 minutes at 37 °C in the dark. After centrifuging, the bacterial suspensions were reconstituted using PBS. A spectrophotometer was used to detect fluorescence anisotropy at excitation and emission wavelengths of 360 nm and 430 nm, respectively. A calculation was made of the fluorescence polarisation (P).[42]

**2.10.3. Determination of potassium ion efflux.** The cells of *B. cereus*, *E. coli*, *S. enterica, and S. flexneri* were first cultivated for 12 h at 37 °C. After being cleaned, the cells were resuspended in phosphate-buffered saline (PBS) with a pH of 7.2 at a density of 1 × 107 cells per mL. One millilitre of the bacterial suspensions containing Ne-SACEO at different concentrations (1/4 MIC, 1/2 MIC, and MIC), along with a control, was then cultured for 2 h at 37 °C. Following centrifugation, Atomic Absorption Spectrometry (AAS) was used to measure the levels of released K+ in the supernatants.[43]

**2.10.4. Determination of the release of 260-nm and 280-nm absorbing materials.** The assessment of leakage of nucleotides was carried out by harvesting cells from the logarithmic growth phase of each bacterial strain. The cells were washed and resuspended in 10 mM PBS (pH 7.2). For varying periods of time, the bacterial strains were incubated with Ne-SACEO. The controls were bacterial strains that were incubated with PBS alone. At 260 nm, the absorbance was measured with a Shimadzu UV-1800 spectrophotometer.[44]

For assessment of protein leakage, after repeating each of the previous procedures, the absorbance at 280 nm was measured. Using albumin from bovine serum (BSA), a standard curve was used to determine the amount of released protein.

**2.10.5. Effect on the growth dynamics.** The experiment to assess the growth dynamics of bacteria under the treatment of Ne-SACEO was started using an initial OD600 of 0.02. Bacterial samples were inoculated into Mueller–Hinton broth and cultivated for eight hours at 37 °C and 200 rpm. Furthermore, 200 μL of dimethyl sulfoxide (DMSO) was used to homogenise different quantities of Ne-SACEO (0.87, 1.30, 1.70, and 2.12 μg $mL^{-1}$) in 1 mL of the standardised bacterial inoculum, which was then added to 20 mL of Mueller–Hinton broth. Before the optical densities were measured, the preparations were kept on an incubator shaker at 200 rpm at 37 °C along with the control in which no oil was added. A spectrophotometer was used to measure the optical density at 600 nm at different intervals, corresponding to every 60 minutes up to 480 minutes following inoculation.[45]

### 2.11. *In silico* analysis

**2.11.1. Homology modelling and structure analysis.** High quality homology models for proteins nor1, omt, and vbs of *A. flavus* were constructed with SWISS-MODEL, using default parameters[46–49] and the putative proteins nor1 (Q00278), omt (Q12120), and vbs (Q12062) of *Aspergillus parasiticus* served as

Open Access Article. Published on 01 2025. Downloaded on 21/06/2026 23:23:45.
This article is licensed under a Creative Commons Attribution-NonCommercial 3.0 Unported Licence.

the template. The quality of the constructed model was assessed with the Ramachandran plot using PROCHECK. The 3D models for the bacterial proteins 7AP3 (P0AGJ9; tyrosine-tRNA ligase) and fabL (P71079; enoyl-[acyl-carrier-protein] reductase) were retrieved from the Alpha fold DB database (AlphaFold Protein Structure Database). The protein models were visualised using Biovia Discovery studio, 2019.

**2.11.2. *In silico* molecular docking.** The putative binding of meta-eugenol with the target proteins was analyzed through *in silico* molecular docking. Initially, the receptor molecules, *i.e.*, nor1, omt, vbs, 7AP3, and fabL were prepared individually by adding polar hydrogens and Kollman charges. Furthermore, the ligand (meta-eugenol) was also prepared for docking in AutoDock Tools 1.5.7. The docking environment was adjusted for the target proteins. Finally, molecular docking was performed using AutoDock vina.exe. The docked complexes were visualized in Biovia Discovery Studio 2019 and UCSF Chimera 1.13.1.[50]

### 2.12. Statistical analysis

All the experiments were performed in triplicate to avoid any errors. Statistical analysis was performed using SAS University Edition software and one-way analysis of variance (ANOVA) with post hoc Tukey and Waller–Duncan tests at 5% confidence ($p < 0.05$). Different lowercase letters (such as *a*, *b*, and *c*) are used to indicate statistical differences within groups.

## 3. Results and discussion

### 3.1. Isolation of essential oils, formation of a combination, and analysis of the chemical profile *via* GC-MS analysis

The EOs were obtained by hydrodistillation of the fresh leaf and clove bud samples separately using the Clevenger apparatus at 90 °C for 3 h. Anhydrous sodium sulfate was used to eliminate excess moisture. Based on the fresh wet weight, the yield was determined to be 0.97% and 0.62% v/w, respectively. To examine the potential of combining these two oils, they were first evaluated independently against bacteria and fungi. They were then mixed in various ratios (leaf: buds-1:1, 1 : 2, 2 : 1, 1 : 3, and 3 : 1). The MIC values were calculated for each of these combinations against *Aspergillus flavus* (0.6, 0.55, 0.75, 0.4, and 0.80 μL $mL^{-1}$), *E. coli* (88.33, 75.66, 90.20, 67.33, and 92.27 ppm), *S. enterica* (72.54, 70.23, 77.97, 64.66, and 78 ppm), *B. cereus* (75, 80.33, 78.97, 72.66, and 84.45 ppm), and *S. flexneri* (78, 77.34, 84.22, 76, and 90.40 ppm). Since the fourth combination, 1 : 3, was determined to be the most effective, it was further chemically characterized using GC-MS (Table 1). The chromatographic analysis by Gas Chromatography-Mass Spectrometry (GC-MS) identified various compounds within the sample based on their retention time. With retention times varying from 22.934 minutes to 39.085 minutes, the study shows a complex blend of 17 different peaks. With a significant 76.05% of the total area, meta-eugenol is the most abundant component in the EOs. Beta-caryophyllene comes in second at 14.93% and humulene and alpha-humulene at 4.77%. Other notable compounds include *cis*-muurola-3,5-diene (0.54%), caryophyllene oxide (1.57%), and humulene epoxide II (0.20%), although in lesser amounts. The other substances, which include 10,10-dimethyl-2,6-bis(methyl), bicycloundecane-5-ol, isocadinene, alpha-selinene, and chavicol, contribute to the sample's minor components, indicating a diverse chemical profile of the analyzed sample (Fig. 1).

### 3.2. Preparation and characterization of the chitosan-cinnamic acid-based nanogel

In this study, low molecular weight chitosan was used as a biocompatible, non-toxic, and biofunctional wall material to encapsulate SACEO. To create a chitosan-cinnamic acid-based nanogel, EDC (1-ethyl-3-(3-dimethyl-aminopropyl-1-carbodiimide)) is used as a zero-length cross-linker. To create an amide bond that promotes acid folding, EDC first integrates with the carboxylic group of cinnamic acid to create an

Table 1 GC-MS analysis of SACEO

| Peaks | Retention time | Area % | Name |
|---|---|---|---|
| 1 | 22.934 | 0.35 | Chavicol |
| 2 | 27.574 | 76.05 | Meta-eugenol |
| 3 | 29.307 | 14.93 | Beta-caryophyllene |
| 4 | 30.641 | 4.77 | Humulene, alpha-humulene |
| 5 | 31.247 | 0.08 | Isocadinene |
| 6 | 32.206 | 0.07 | Alpha-selinene |
| 7 | 32.630 | 0.12 | (*E*,*E*)-Alpha-farnesene |
| 8 | 33.135 | 0.54 | *cis*-Muurola-3,5-diene |
| 9 | 34.335 | 0.19 | Humulene epoxide II |
| 10 | 34.528 | 0.28 | Cyclohexane, 1,5-dimethyl-2,3-divinyl- |
| 11 | 35.384 | 0.27 | Caryolan-8-ol |
| 12 | 35.606 | 1.57 | Caryophyllene oxide |
| 13 | 36.060 | 0.10 | *cis*-4(14),5-muuroladiene |
| 14 | 36.648 | 0.20 | Humulene epoxide II |
| 15 | 37.767 | 0.19 | Bicyclo[7.2.0] undecane-5-ol, 10,10-dimethyl-2,6-bis(methyl) |
| 16 | 38.505 | 0.14 | Androstan-1.7-one, 3-ethyl-3-hydroxy-, (5. alpha.)- |
| 17 | 39.085 | 0.15 | Caryophyllene oxide |


© 2026 The Author(s). Published by the Royal Society of Chemistry

Open Access Article. Published on 01 2025. Downloaded on 21/06/2026 23:23:45.
This article is licensed under a Creative Commons Attribution-NonCommercial 3.0 Unported Licence.

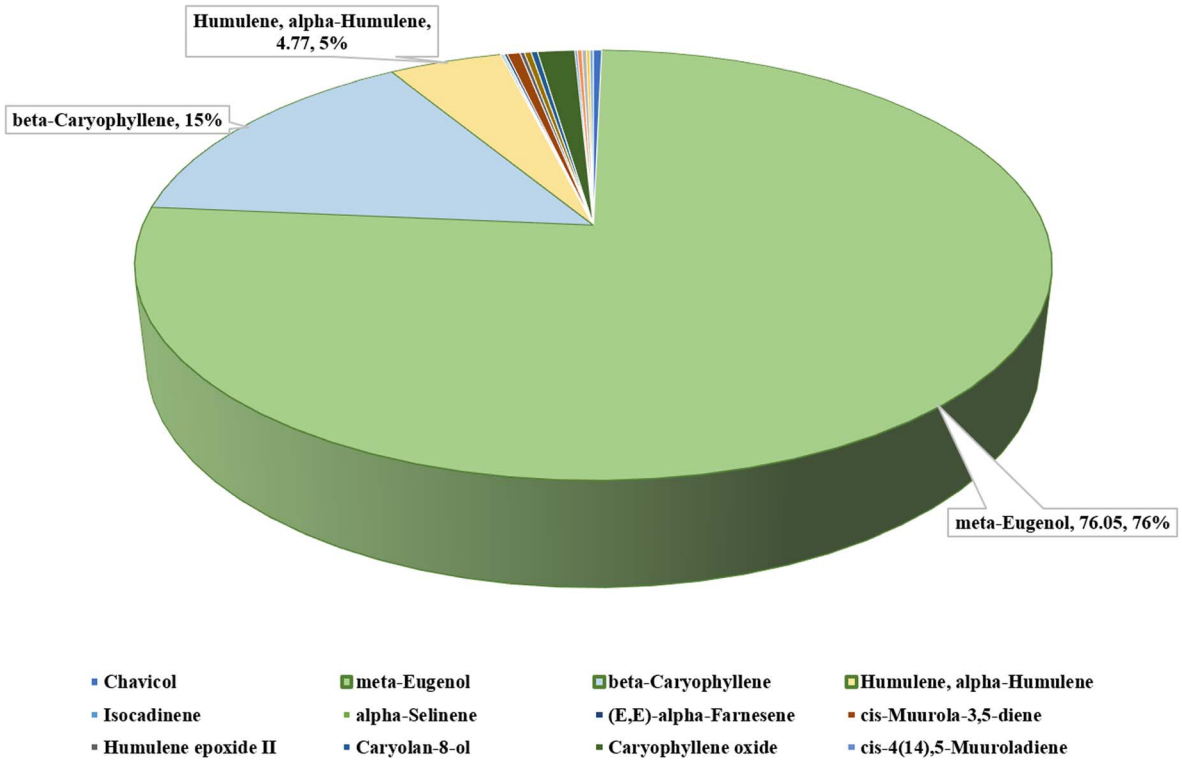


Fig. 1 GC-MS profile of SACEO.

intermediate, which subsequently reacts with the amino group of chitosan. The EDC-mediated binding of non-polar cinnamic acid to the chitosan polymer causes self-aggregation in a polar environment, resulting in the formation of an integrated spherical nanogel with a hydrophilic shell (chitosan) and a hydrophobic core (cinnamic acid). An oil-in-water emulsion is used to encapsulate SACEO within this hydrophobic core, and then sonication is used to produce a nanoscale particle size.[51]

**3.2.1. Characterization of nanoparticles.** ATR-FTIR and Dynamic Light Scattering (DLS) were used to characterize the synthesized nanoparticles. The functional group composition of chitosan, chitosan nanoparticles (CSNPs), *Syzygium aromaticum* combination essential oil (SACEO), and the nano-encapsulated essential oil (Ne-SACEO) was analyzed by ATR-FTIR analysis. The results of ATR-FTIR analysis establish the successful synthesis of nanoparticles and also revealed that the SACEO was successfully incorporated in the chitosan-cinnamic acid nanomatrix.

Each spectrum provides insight into the structural changes and chemical interactions taking place during the synthesis and encapsulation of nanoparticles.[52] The broad peak at 3366 $cm^{-1}$ in the chitosan FTIR spectrum (red line) represents the O–H and N–H stretching of the hydroxyl and amine groups. Aliphatic C–H stretching is indicated by a peak at 2898 $cm^{-1}$, whereas C═O stretching is responsible for the amide I peak at 1644 $cm^{-1}$. The polysaccharide backbone, which is characteristic of chitosan, is confirmed by a peak at 1380 $cm^{-1}$ (C–N stretching or $CH_3$ bending) and 1026–896 $cm^{-1}$ (C–O stretching and saccharide structure). The O–H/N–H portion of the CSNP spectra (green line) shifts to 3340 $cm^{-1}$, suggesting hydrogen bonding and interactions with EDC and cinnamic acid. Imine (C═N) production or cross-linking is suggested by the new peaks at 2101 and 1796 $cm^{-1}$. The production of C–N and C–O–C bonds is represented by the bands at 1671 and 1222 $cm^{-1}$, which validate the successful creation of nanoparticles. The SACEO spectrum (blue line) displays C═C aromatic stretching at 1606 $cm^{-1}$, a wide O–H peak at 3322 $cm^{-1}$, and C–H stretches at 2966, 2929, and 2859 $cm^{-1}$. Peaks in the fingerprint region (1500–600 $cm^{-1}$) confirm the presence of meta-eugenol and other eugenol derivatives. Strong interaction and effective encapsulation are confirmed by the Ne-SACEO spectrum (yellow line), which overlaps chitosan and SACEO characteristics with the key peaks located at 3369, 2933, 1633, 1460, 1242, 1072, and 1029 $cm^{-1}$. These results validate the successful encapsulation and stable configuration of SACEO in the nanomatrix (Fig. 2a).

The size distribution and surface charge of free chitosan nanoparticles (CSNPs) and *S. aromaticum* combination essential oil-loaded nanoparticles (Ne-SACEO) were assessed using zeta potential and dynamic light scattering (DLS) techniques. A sharp, narrow peak centered at 140–150 nm was visible in the DLS profile of free CSNPs, suggesting a homogeneous particle size that has significant monodispersity. The development of evenly distributed, non-aggregated nanoparticles was further validated by the intensity peak surpassing 80%. The Ne-SACEO formulation showed a size distribution centered at 160–180 nm, indicating a slight increase in the particle size upon encapsulation of SACEO. This change signifies that the oil has been

Open Access Article. Published on 01 2025. Downloaded on 21/06/2026 23:23:45.
This article is licensed under a Creative Commons Attribution-NonCommercial 3.0 Unported Licence.

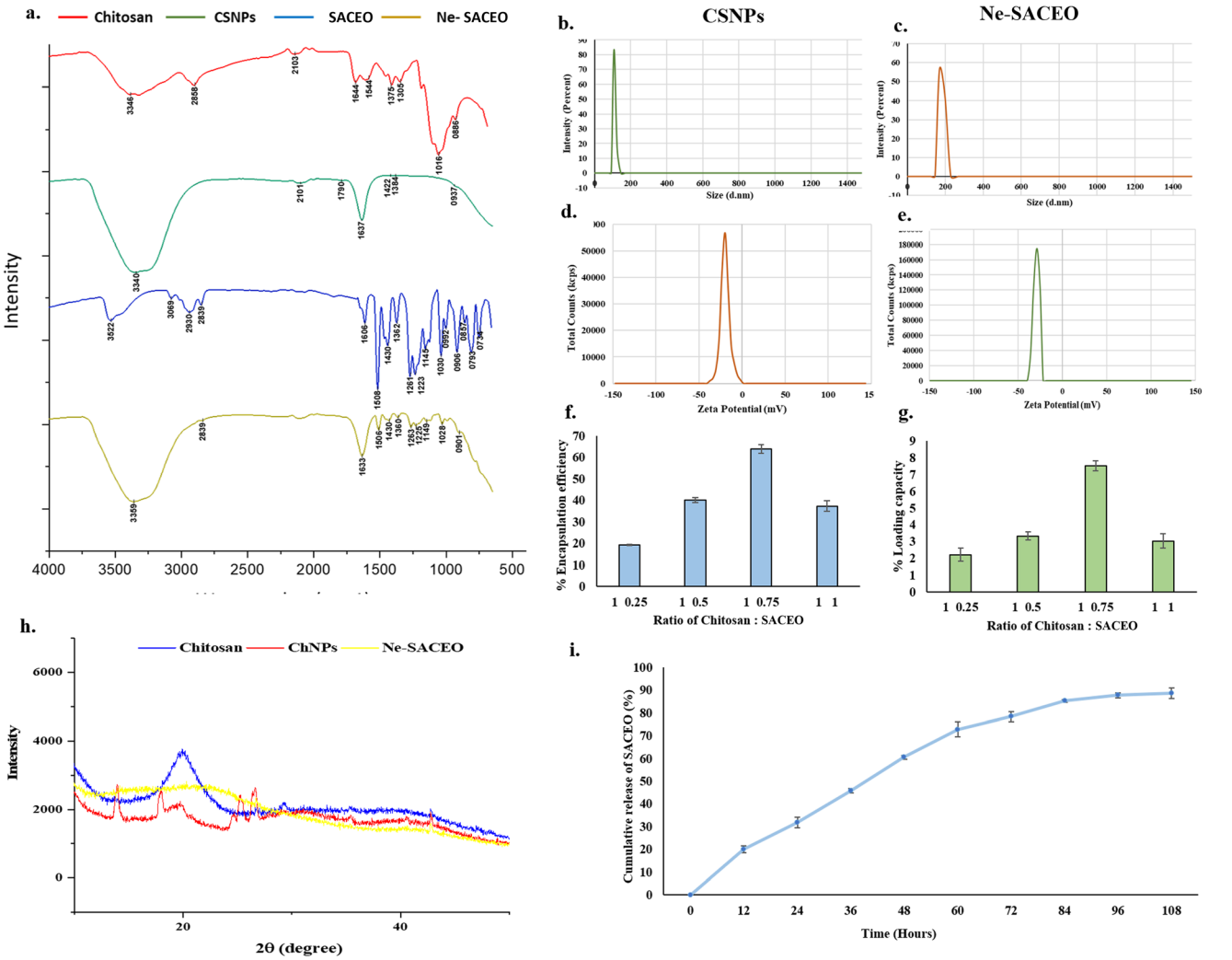


Fig. 2 Characterization of the synthesized nanoparticle Ne-SACEO: (a) ATR-FTIR spectra showing characteristic peaks, (b) dynamic light scattering of CSNPs, (c) dynamic light scattering of Ne-SACEO, (d) zetapotential of CSNPs, (e) zetapotential of Ne-SACEO, (f) percentage encapsulation efficiency, (g) percentage loading capacity, (h) XRD analysis and (i) *in vitro* release.

successfully integrated into the chitosan matrix, and the continuous sharpness in the peak shows that the formulation is stable and homogeneous[53] (Fig. 2b and c).

The measurements of zeta potential showed that free CSNPs had a significant negative surface charge of about −45 mV, which suggests that electrostatic repulsion ensures excellent colloidal stability. Following encapsulation, the zeta potential of Ne-SACEO considerably reduced between −35 and −40 mV. This decrease is probably driven by oil components partially covering the surface, although the results are still within the extremely stable range (more than ±30 mV)[54] (Fig. 2d and e).

The successful synthesis and encapsulation of SACEO into chitosan nanoparticles is confirmed by the DLS and zeta potential data taken into account. This results in a stable and uniform nanodispersion that may find use in antibacterial or food preservation systems.

The XRD pattern shows distinct differences in crystallinity among chitosan, ChNPs, and Ne-SACEO. The native chitosan sample exhibits a sharp and intense diffraction peak characteristic of its semi-crystalline nature. Upon nanoparticle formation, these peaks broaden and their intensity decreases, indicating a loss of crystallinity and amorphization of the chitosan matrix. In the Ne-SACEO sample, the diffraction pattern becomes even more diffused with reduced peak intensity, suggesting further disruption of the chitosan crystalline structure due to encapsulation of SACEO. The decreased crystallinity arises from intermolecular hydrogen bonding between chitosan and essential oil components, which interfere with the regular ChNP alignment (Fig. 2h).

**3.2.2. Encapsulation efficiency, loading capacity, and *in vitro* release.** The analysis of encapsulation potential reveals that as the ratio of chitosan to SACEO increases from 1 : 0.25 to 1 : 0.75, the Encapsulation Efficiency (EE%) increases as well, reaching a peak of roughly 63–64%. This suggests improved encapsulation up to a certain ratio of SACEO and nanoparticles. At a 1 : 1 ratio, however, the EE% falls abruptly to about 37–38%, indicating either chitosan saturation or ineffective encapsulation brought on by an excess of oil or aggregation of


© 2026 The Author(s). Published by the Royal Society of Chemistry

Open Access Article. Published on 01 2025. Downloaded on 21/06/2026 23:23:45. This article is licensed under a Creative Commons Attribution-NonCommercial 3.0 Unported Licence.

nanoparticles. Additionally, the loading capacity (LC%) exhibits a similar trend. From 1 : 0.25 to 1 : 0.75, the LC% increases gradually until it reaches a maximum of 7.5–7.6%, which suggests increased SACEO loading. The LC% drops to 3.2–3.3% at the 1 : 1 ratio, indicating that chitosan cannot efficiently encapsulate excess oil after a specific threshold.[55]

In summary, the best ratio for nanoencapsulation, yielding the highest EE% and LC%, is 1 : 0.75 chitosan to SACEO (Fig. 2f and g). The performance is decreased by ratios above or below this ideal value, highlighting the crucial role that stoichiometric balance plays in stable encapsulation and nanoparticle production.

The release profile of SACEO demonstrates a sustained and controlled release pattern. An initial burst release of approximately 20–25% occurs within the first 12 hours, followed by a gradual increase to around 60% at 48 hours. The release rate subsequently slows, reaching about 80% at 84 hours and saturating near 90% after 100 hours. The initial rapid release likely corresponds to the release of surface-associated SACEO, while the slower phase is governed by diffusion through the polymeric matrix (Fig. 2i).

### 3.3. Free radical scavenging activity demonstrated by nanoencapsulated SACEO

The DPPH and ABTS free radical scavenging assays were used to evaluate the antioxidant activity of Ne-SACEO. The existence of strong antioxidant components in the formulation was confirmed by both tests, resulting in a concentration-dependent increase in free radical inhibition. Ne-SACEO showed a substantial increase in inhibition above 0.02 μL $mL^{-1}$ in the DPPH assay, increasing from 10.01% at 0.005 μL $mL^{-1}$ to 64.84% at 0.035 μL $m^{-1}$. This can be explained by meta-eugenol, a crucial phenolic molecule that lowers DPPH radicals by serving as a hydrogen donor. The calculated $IC_{50}$ was around 0.028 μL $mL^{-1}$ (Fig. 3a).

Ne-SACEO showed significantly stronger action in the ABTS assay, with inhibition increasing from 18.1% at 0.001 μL $mL^{-1}$ to 71.21% at 0.007 μL $mL^{-1}$. $IC_{50}$ was estimated to be 0.0042 μL $mL^{-1}$ (Fig. 3b). The improved solubility and interaction of the encapsulated components with both hydrophilic and lipophilic radicals may be the cause of the increased efficacy in the ABTS experiment. These findings imply that the antioxidant properties of EOs are improved by nanoencapsulation, hence reinforcing their use in food preservation formulations.

### 3.4. Inhibition of growth of *A. flavus* and aflatoxin $B_1$: determination of MIC and MAIC

*A. flavus* was used as a test fungus to investigate the antifungal and anti-aflatoxigenic properties of *S. aromaticum* essential oils from leaves, buds, and their combination in both free and nanoencapsulated forms (Ne-SACEO) (Fig. 4a–c). At 0.3 μL $mL^{-1}$, leaf oil demonstrated a nearly 100% reduction of aflatoxin B1 ($AFB_1$) synthesis but a moderate inhibition of the mycelial dry weight (MDW), suggesting selective suppression of the secondary metabolism. Because of its different composition of bioactives, bud oil had greater potency, almost completely inhibiting both MDW and AFB1 at lower dosages.

The combination of leaf and bud oil enhanced both the antifungal and antiaflatoxigenic activity and resulted in MIC and MAIC values of 0.4 and 0.2 μL $mL^{-1}$. SACEO's effectiveness was further enhanced by the synergistic effects of several of its ingredients, including eugenol, meta-eugenol, and β-caryophyllene. At lower concentrations, the combination oil (SACEO) showed increased activity, notably in its nanoencapsulated form (Ne-SACEO). Ne-SACEO demonstrated enhanced fungal growth and toxin production suppression because the active compounds were more soluble, stable, and bioavailable. The MIC and MAIC values were determined to be 0.35 and 0.15 μL $mL^{-1}$, respectively which is significantly lower than those of the synthetic antifungal preservative benzoic acid (MIC & MAIC, 1.25 μL $mL^{-1}$) and sorbic acid (MIC & MAIC, 1.25 μL $mL^{-1}$).[56] By enhancing dispersion in aqueous media, shielding volatile substances, permitting sustained release, and promoting deeper cell wall penetration, nanoencapsulation dramatically increased bioactivity, enabling Ne-SACEO to become a stable, strong, and efficient antifungal and anti-aflatoxigenic agent.[57]

### 3.5. Functional principle behind the impediment in fungal growth and toxin production

**3.5.1. Alteration in the function of the plasma membrane: decrease in ergosterol content and leakage of cytoplasmic components.** The assessment of function principles underlying the action of Ne-SACEO against *A. flavus* and aflatoxin $B_1$

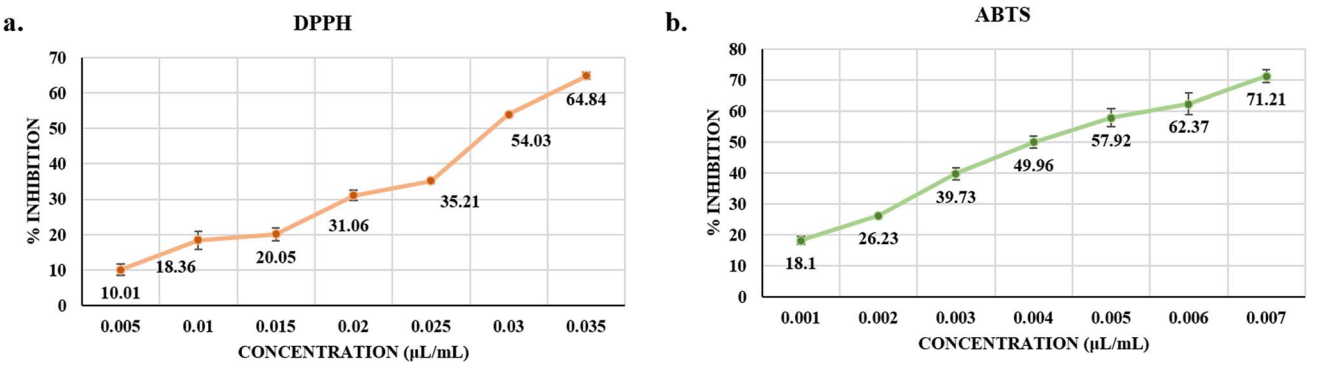


Fig. 3 Free radical scavenging potential of Ne-SACEO: (a) DPPH assay and (b) ABTS assay.

Open Access Article. Published on 01 2025. Downloaded on 21/06/2026 23:23:45.
This article is licensed under a Creative Commons Attribution-NonCommercial 3.0 Unported Licence.

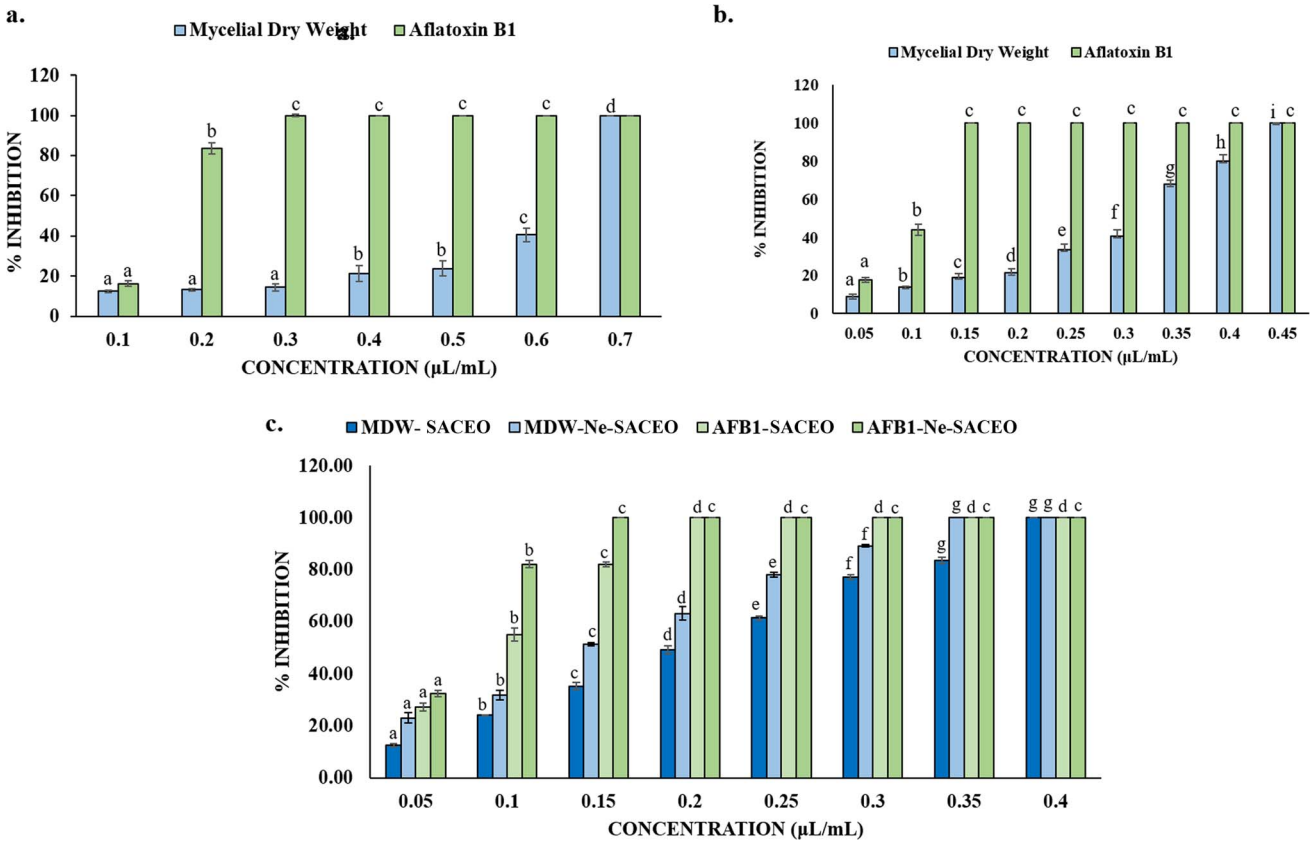


Fig. 4 Antifungal and antiaflatoxigenic activity of (a) SALEO, (b) SABEO, (c) SACEO, and Ne-SACEO.

resulted in significant revelations. The primary target of the nanoencapsulated oil can be the plasma membrane, resulting in the death and toxin inhibition.

The ergosterol assay shows that Ne-SACEO significantly lowers the amount of ergosterol in the *A. flavus* plasma membrane in a concentration-dependent manner. Ergosterol is only slightly inhibited at $\frac{1}{4}$ MIC, while a significant reduction of approximately 40% in its content can be observed at $\frac{1}{2}$ MIC. Ergosterol content is entirely suppressed at the MIC level, indicating a serious disturbance of the membrane structure (Fig. 5a). This implies that treatment of Ne-SACEO may lead to destabilization of the membrane and compromise fungal cell viability by interfering with ergosterol biosynthesis genes and enzymes.[58] Ergosterol is an essential fungal sterol that keeps membranes functioning, fluid, and intact, making the fungal cell more resistant to external stress. The damage to ergosterol can lead to damaged cell integrity and ultimately cause cell death.

The ion leakage experiment demonstrates that extracellular levels of $K^+$ and $Mg^{2+}$ ions increase significantly after treatment with Ne-SACEO, with $K^+$ leaching out more than $Mg^{2+}$ at all doses. Minimal leakage in the control (CNT) suggests that the membranes are intact. However, a dose-dependent increase in the ion content is observed as concentrations increase from $\frac{1}{4}$ MIC to MIC (Fig. 5b). This implies that Ne-SACEO impairs the selective permeability of the membrane, causing necessary internal ions to leak out. This type of ionic imbalance can affect cellular signaling, osmoregulation, and enzyme activity, all of which can lead to the death of fungal cells.[59]

The release of intracellular components that absorb at 260 and 280 nm, respectively, for nucleic acids and proteins, suggests that there is a substantial amount of cellular leakage after Ne-SACEO treatment. From the control to MIC, the absorbance gradually increases, with MIC exhibiting the highest leakage (absorbance −0.42 at 260 nm and 0.40 at 280 nm) (Fig. 5c). This implies that Ne-SACEO affects deeper cellular components in addition to the outer membrane, causing the release of big macromolecules like proteins, RNA, and DNA.[59] The idea that the antifungal action of Ne-SACEO comprises significant harm to both cytoplasmic and organelle membranes is supported by the leakage of these macromolecules, which also verifies significant membrane disruption.

**3.5.2. Altered mitochondrial health: depolarization of the mitochondrial membrane.** The treatment of Ne-SACEO has a considerable impact on the mitochondrial membrane potential (MMP) of *A. flavus*. There is a concentration-dependent decrease in MMP, with inhibition of approximately 15% at $\frac{1}{4}$ MIC, 28% at $\frac{1}{2}$ MIC, and more than 40% at MIC (Fig. 5d). Mitochondrial membrane potential (MMP) is a key electrochemical gradient across the inner mitochondrial membrane, crucial for driving the synthesis of ATP *via* oxidative phosphorylation. Energy metabolism and mitochondrial


© 2026 The Author(s). Published by the Royal Society of Chemistry

Open Access Article. Published on 01 2025. Downloaded on 21/06/2026 23:23:45.
This article is licensed under a Creative Commons Attribution-NonCommercial 3.0 Unported Licence.

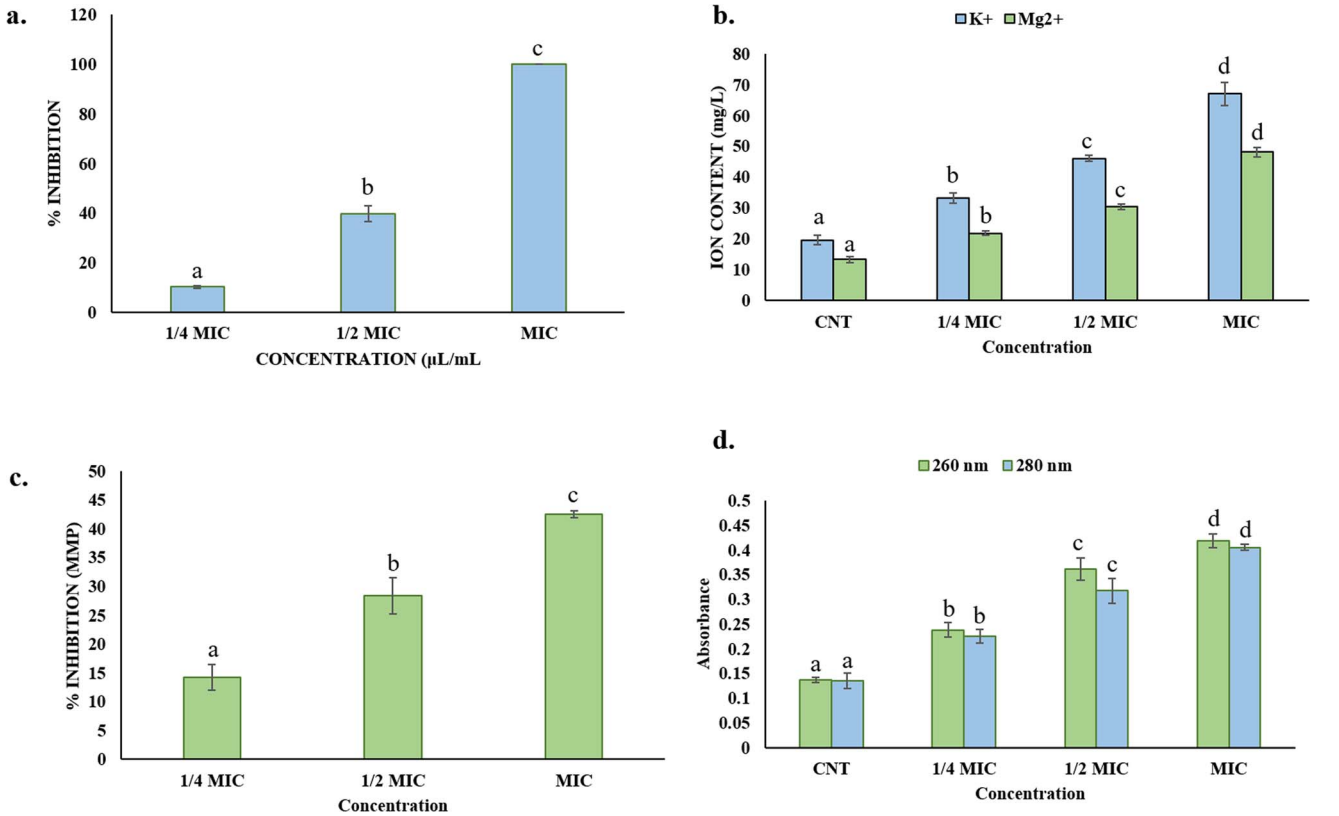


Fig. 5 Antifungal mechanism of action of Ne-SACEO against *A. flavus*: (a) percentage inhibition of ergosterol content, (b) leakage of cellular ions, (c) percentage inhibition of mitochondrial membrane potential, and (d) leakage of 260 nm and 280 nm absorbing materials.

activity in eukaryotic creatures depend on this potential, which is maintained by the electron transport chain. This disruption may have been driven by the production of ROS or damage to mitochondrial membranes from Ne-SACEO. Loss of MMP contributes to the antifungal action by limiting ATP generation and triggering apoptotic-like pathways. The activity of phenolic components (meta-eugenol), which may damage mitochondrial membranes and encourage the production of reactive oxygen species (ROS), is probably the cause of this impairment.[60] The proton gradient necessary for ATP synthesis collapses as a result of such oxidative stress and membrane depolarisation, leading to cell death. Therefore, mitochondrial impairment represents the key mode of antifungal action for Ne-SACEO, highlighting its potential as a bioactive agent targeting fungal energy metabolism.

### 3.6. Action of Ne-SACEO against foodborne bacteria and assessment of MIC

The ability of various *S. aromaticum* essential oil compositions to combat four main foodborne pathogens, including both Gram-positive (*B. cereus*) and Gram-negative (*E. coli*, *S. enterica*, and *S. flexneri*) species was investigated in this study. The MTT assay revealed that the MIC of bacteria was found to be between 60 to 120 ppm for leaf and bud oils. However, compared to the individual leaf (SALEO) and bud oils (SABEO), the combination oil (SACEO) showed better efficacy, likely due to synergistic interactions among its phytochemical constituents. The nanoencapsulated combination essential oil (Ne-SACEO) demonstrated the best antibacterial action among the studied oils, with the lowest MIC values across all strains: *B. cereus*, *E. coli*, *S. enterica*, and *S. flexneri* with MICs of around 57, 55, 50, and 64, respectively (Fig. 6a). The antibacterial activity of the Ne-SACEO was comparable to and more promising than that of the standard neomycin sulfate. Nanoencapsulation, which increases solubility, shields volatile bioactives from deterioration, permits sustained release, and allows deeper cellular penetration, is responsible for this increased efficacy.

Nanoencapsulation enhances penetration, especially in Gram-negative bacteria with outer membranes rich in lipopolysaccharides. It overcomes the outer membrane barrier of Gram-negative strains and effectively targets the thick peptidoglycan layer of Gram-positive *B. cereus*. The small particle size of Ne-SACEO enables it to bypass this barrier, destabilize the membrane, and increase intracellular accumulation. The superior efficacy of Ne-SACEO highlights the importance of both phytochemical synergy and the delivery system in antimicrobial applications.

### 3.7. Functional principle behind the inhibition of bacterial growth

**3.7.1. Effect on the plasma membrane integrity.** The experiments conducted to elucidate the mechanism of action of

Open Access Article. Published on 01 2025. Downloaded on 21/06/2026 23:23:45.
This article is licensed under a Creative Commons Attribution-NonCommercial 3.0 Unported Licence.

Ne-SACEO against different bacterial strains revealed the possible sites of action.

The Rhodamine 123 (Rh123) fluorescence assay was used to determine the manner in which Ne-SACEO affects the membrane potential of bacteria. As Ne-SACEO concentrations increased, a noticeable, dose-dependent drop in fluorescence intensity was observed for *S. enterica*, *B. cereus*, *S. flexneri*, and *E. coli*, suggesting a gradual decrease of the membrane potential (Fig. 6b). The control groups exhibited strong fluorescence, suggesting an intact membrane under untreated conditions. On the other hand, cells exposed to Ne-SACEO at MIC levels showed the least amount of fluorescence, indicating a significant depolarisation of the membrane. Interestingly, *S. flexneri* and *B. cereus* showed more fluorescence loss and were thus more sensitive. Rh123 is a cationic dye that binds to living cells whose membranes have intact proton gradients. Dye uptake is inhibited when this gradient is disturbed, which is frequently the result of membrane injury. The bioactive components, such as eugenol, meta-eugenol, and other phenolics found in essential oils, are known to integrate into bacterial membranes, causing leakage of ions and collapse of the membrane potential. This interrupts ATP synthesis and other energy-dependent processes, leading to metabolic failure and cell death. Thus, the observed reduction in fluorescence strongly supports the hypothesis that Ne-SACEO compromises bacterial viability through membrane depolarization, contributing to its antibacterial potency.

Furthermore, the impact of Ne-SACEO on membrane fluidity was assessed by measuring the fluorescence polarization index. In comparison to the control, a consistent and dose-dependent rise in the polarisation index for *E. coli*, *S. enterica*, *B. cereus*, and *S. flexneri* was recorded when Ne-SACEO concentrations increased (from $\frac{1}{4}$ MIC to MIC). This shows that Ne-SACEO increases membrane rigidity by efficiently reducing membrane fluidity (Fig. 6c). The effect was more noticeable in *B. cereus* and S. *enterica*, indicating that they are more vulnerable to treatments that target membranes.[61]

The DPH probe is embedded in the hydrophobic core of membranes; in more fluid membranes, it rotates freely, resulting in less polarisation. Bioactive components integrate into the lipid bilayer and disrupt the orderly arrangement of phospholipids. The polarisation index increases as Ne-SACEO breaks down lipid packing, which reduces DPH's rotational freedom. Energy production, transport, and membrane functions are all hampered by this rigidification. These results offer strong evidence that the bacterial membrane structural and functional disruption mediates Ne-SACEO's antibacterial effect.

Additionally, when Ne-SACEO was administered to all four bacterial species, the measurement of ion leakage from bacterial cells resulted in a dose-dependent rise in potassium ion concentration. The bacteria with the largest $K^+$ ion leakage at MIC were *E. coli*, followed by *S. enterica*, *B. cereus*, and *S. flexneri* (Fig. 6d). Potassium, a necessary intracellular ion, leaks when the membrane's integrity is compromised. Ne-SACEO disrupts the bacterial cytoplasmic membrane, changing its permeability and ultimately leading to cell death and dysfunction, as indicated by the increased ion efflux. Potassium ions are necessary for osmotic balance, enzyme activity, and cell functions ($K^+$). The membrane's phospholipid bilayer, which is selectively permeable, frequently keeps $K^+$ inside the cell cytoplasm. Ne-SACEO enters the lipid bilayer and increases the fluidity and permeability of the membrane when it interacts with it, especially through its hydrophobic constituents. As a result, $K^+$ ions passively leak into the extracellular space. An ionic imbalance

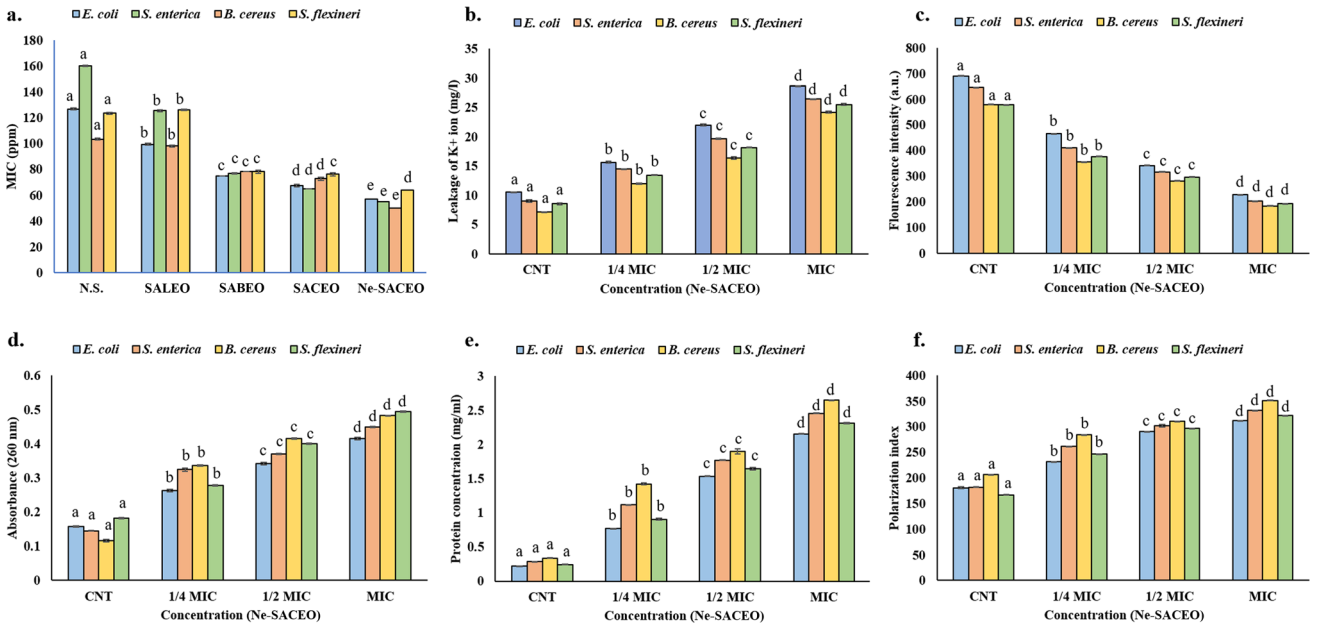


Fig. 6 Ne-SACEO against bacterial pathogens: (a) MIC of neomycin sulfate (N.S.), SALEO, SABEO, SACEO, and Ne-SACEO; antibacterial mechanism of action: (b) membrane potential, (c) membrane fluidity, (d) leakage of K+ ions, (e) leakage of 260 nm absorbing materials and (f) protein leakage.


© 2026 The Author(s). Published by the Royal Society of Chemistry

Open Access Article. Published on 01 2025. Downloaded on 21/06/2026 23:23:45.
This article is licensed under a Creative Commons Attribution-NonCommercial 3.0 Unported Licence.

disrupts metabolic homeostasis, prevents enzyme activity, and ultimately leads to cell death.[62]

The absorbance at 260 nm was used to quantify the amount of nucleic acids (DNA/RNA) that leaked from bacterial cells after they were exposed to Ne-SACEO. From $\frac{1}{4}$ MIC to MIC, absorbance gradually increases, with *B. cereus* and *S. enterica* exhibiting slightly higher leakage than the others. This implies that Ne-SACEO can damage cell membranes profoundly and irreversibly by allowing big intracellular macromolecules to escape. Significant damage to the membrane is indicated by the presence of nucleic acids (DNA and RNA) in the extracellular environment. Ne-SACEO most likely causes formation of pores or may also lead to the complete cytoplasmic membrane damage, which permit big intracellular molecules like DNA and RNA to move into the extracellular space (Fig. 6e).

Protein leakage from damaged membranes is confirmed by the fact that protein concentration in the extracellular environment increases with Ne-SACEO concentration. *S. enterica* exhibits the highest protein release at MIC concentration, indicating that it is highly susceptible to membrane disruption by Ne-SACEO (Fig. 6f). By triggering metabolic breakdown and antibacterial effects, the leakage of essential cytoplasmic proteins supports membrane destruction as the main mode of action. As mentioned earlier, healthy bacterial membranes are impervious to large macromolecules like cytoplasmic proteins, lipids, and nucleic acids. Their discharge following Ne-SACEO treatment confirms the loss of structural integrity of the membrane. This might occur as a result of the direct interaction between oil components and protein transport pathways, the oxidation of membrane proteins, or the degradation of membrane lipids. Additionally, it has been shown that phenols like meta-eugenol denature proteins and disrupt the cellular redox balance, which may damage membrane-attaching structural proteins or enzymes and cause them to split and leak out. This leakage disrupts vital processes, including metabolism and repair systems, ultimately leading to cell death.

**3.7.2. Alteration in the growth dynamics.** The antibacterial efficacy of the tested essential oil was evaluated against four foodborne pathogens—*S. enterica*, *B. cereus*, *E. coli*, and *S. flexneri*—at varying concentrations ($\frac{1}{4}$ MIC, $\frac{1}{2}$ MIC, and MIC) over a time course of 480 minutes. Optical density (OD) readings were recorded at 60 minute intervals to monitor the bacterial growth kinetics in the presence and absence of the essential oil (Fig. 7a–d).

The control group exhibited a consistent rise in O.D. for *S. enterica*, suggesting significant bacterial growth. A slower increase in OD over time, however, indicated partial growth inhibition brought on by treatment with $\frac{1}{4}$ MIC and $\frac{1}{2}$ MIC doses (Fig. 7a). Interestingly, OD readings remained almost constant and near zero during the testing period, indicating that the MIC concentration completely inhibited bacterial growth. A similar pattern was seen for *B. cereus*, however, the bacteria seemed to be a little more resilient to the smaller essential oil concentrations. However the $\frac{1}{4}$ MIC and $\frac{1}{2}$ MIC treatments slowed down the growth, but did not completely suppress bacterial growth. However, the MIC treatment successfully stopped the growth of

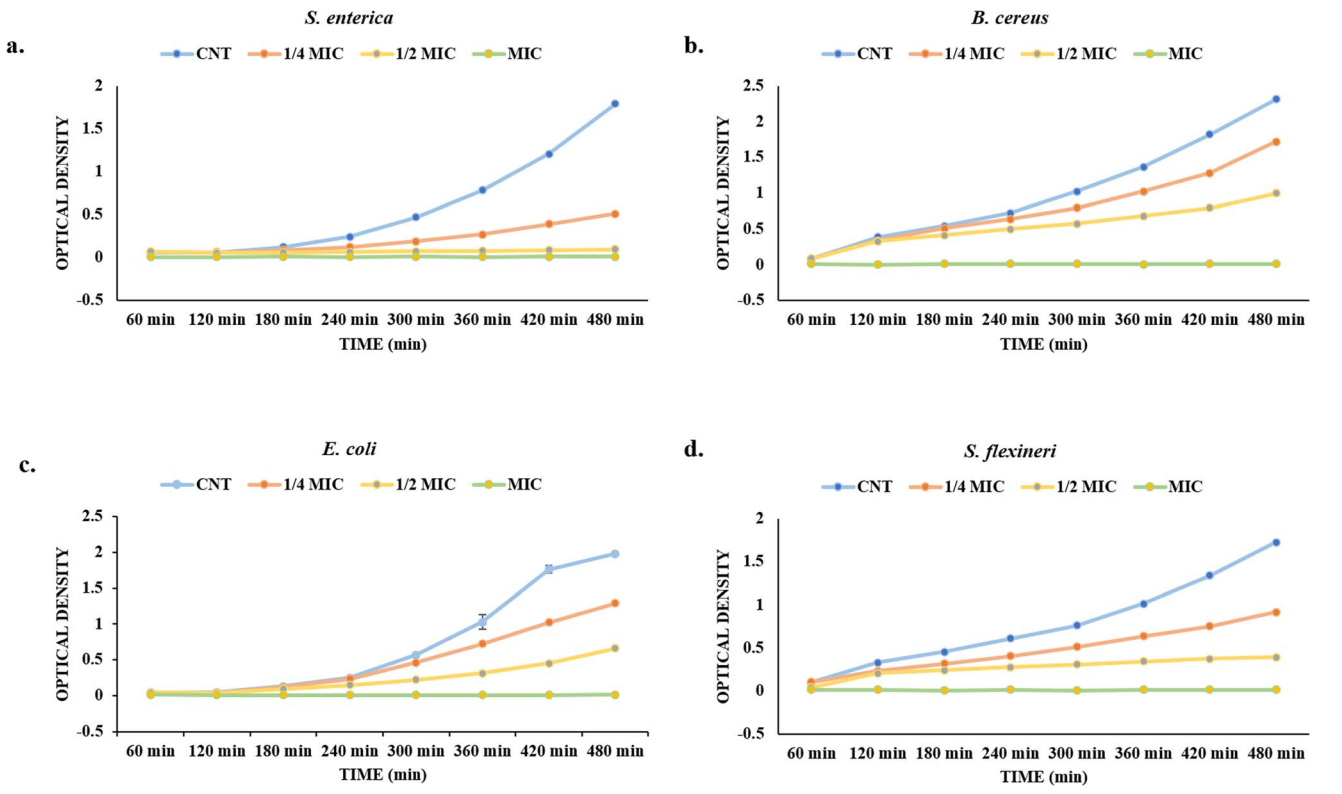


Fig. 7 Growth curve under different treatment conditions (CNT, $\frac{1}{4}$ MIC, $\frac{1}{2}$ MIC, and MIC): (a) *S. enterica*, (b) *B. cereus*, (c) *E. coli*, and (d) *S. flexneri*.

Open Access Article. Published on 01 2025. Downloaded on 21/06/2026 23:23:45.
This article is licensed under a Creative Commons Attribution-NonCommercial 3.0 Unported Licence.

Table 2 Molecular docking of meta-eugenol with fungal and bacterial proteins

| S. no. | Dock complex | 2D-map of interacting residues | Types of interaction and interacting residues | Binding energy (kcal $mol^{-1}$) |
|---|---|---|---|---|
| 1 | 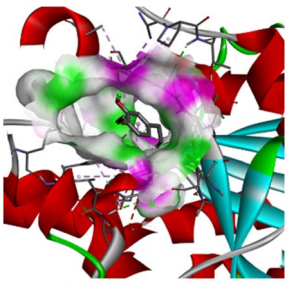 Afnor1- meta-eugenol | 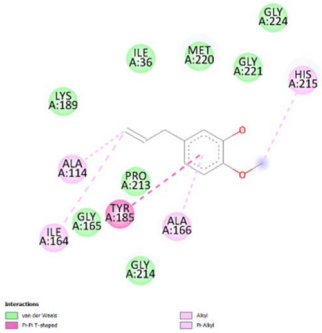 | • Van der waals ($I^{36}$, $L^{189}$, $G^{165}$, $P^{213}$, $G^{214}$, $M^{220}$, $G^{221}$, $G^{224}$)<br>• π–π ($Y^{185}$)<br>• Alkyl and π-alkyl ($A^{114}$, $I^{164}$, $A^{166}$, $H^{215}$) | −4.7 |
| 2 | 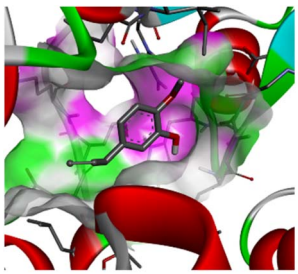 Afomt1- meta-eugenol | 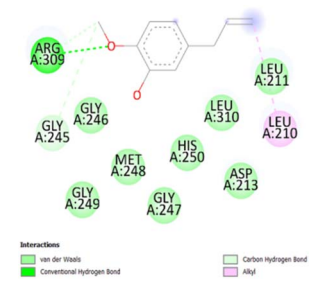 | • Van der waals ($D^{213}$, $L^{211}$, $G^{247}$, $M^{248}$, $G^{249}$, $H^{250}$)<br>• Conventional H-bond ($R^{309}$)<br>• Alkyl ($L^{210}$)<br>• Carbon hydrogen bond ($G^{245}$) | −5.5 |
| 3 | 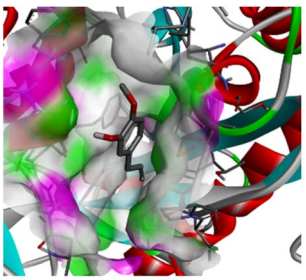 Afvbs1- meta-eugenol | 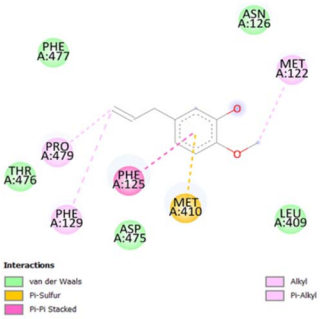 | • Van der waals ($N^{126}$, $L^{409}$, $D^{475}$, $T^{476}$, $F^{477}$)<br>• π–π ($F^{125}$)<br>• Alkyl and π-alkyl ($M^{122}$, $P^{479}$, $F^{129}$)<br>• π-sulfur ($M^{410}$) | −4.8 |
| 4 | 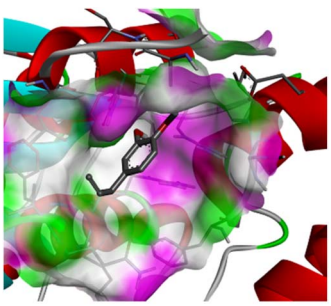 7AP3- meta-eugenol | 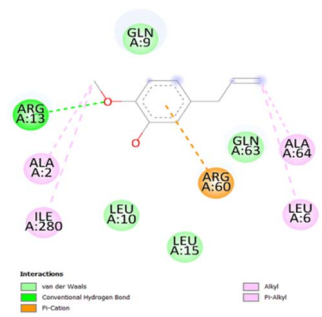 | • Van der waals ($Q^{9}$, $L^{10}$, $L^{15}$, $Q^{63}$)<br>• Alkyl and π-alkyl ($A^{2}$, $L^{6}$, $A^{64}$, $I^{280}$)<br>• Conventional H-bond ($R^{13}$)<br>• π-cation ($R^{60}$) | −5.2 |
| 5 | | | • Van der waals ($T^{145}$, $I^{193}$, $S^{197}$) | −6.3 |


© 2026 The Author(s). Published by the Royal Society of Chemistry

Open Access Article. Published on 01 2025. Downloaded on 21/06/2026 23:23:45.
This article is licensed under a Creative Commons Attribution-NonCommercial 3.0 Unported Licence.

Table 2 (*Contd.*)

| S. no. | Dock complex | 2D-map of interacting residues | Types of interaction and interacting residues | Binding energy (kcal $mol^{-1}$) |
|---|---|---|---|---|
| | fabL- meta-eugenol | | • Alkyl and π-alkyl ($I^{20}$, $Y^{147}$, $Y^{157}$, $A^{198}$, $V^{201}$, $F^{204}$, $I^{207}$)<br>• Conventional H-bond ($T^{195}$) | |

bacteria, keeping the OD values almost at initial levels (Fig. 7b). In the case of *E. coli*, bacterial growth in the control group increased gradually over time and almost stabilized at 480 min, unlike other bacteria (Fig. 7c). The $\frac{1}{4}$ MIC treatment allowed for moderate growth, while the $\frac{1}{2}$ MIC considerably suppressed it. The MIC concentration was highly effective, completely halting bacterial growth as indicated by consistently low OD readings throughout the assay. However, in treated samples, no steadiness in the growth curve was observed, which can be attributed to an increase in growth time and thus slow growth. Interestingly, *S. flexneri* demonstrated the highest sensitivity among the tested pathogens. Even at $\frac{1}{2}$ MIC, bacterial growth was significantly inhibited, with only a gradual increase in OD observed (Fig. 7d). The MIC concentration entirely prevented growth, resulting in a flat OD curve throughout the experiment. This suggests a strong antibacterial potential of the essential oil against *S. flexneri*, even at sub-inhibitory concentrations.

Collectively, these findings confirm that the essential oil exhibits dose-dependent antibacterial activity, with the MIC concentration being uniformly effective in suppressing bacterial growth across all tested strains. The differential response at sub-MIC levels further indicates that the susceptibility varies by species, positioning this natural product as a promising candidate for the control of foodborne bacterial pathogens.

### 3.8. *In silico* analysis

**3.8.1. Homology modelling and molecular docking.** High-quality homology models of the target proteins were successfully generated. The 3D models were validated by the Ramachandran plot analysis, which confirmed the stereochemical quality and reliability of the predicted structures. The target proteins exhibited typical α/β structural folds, characteristic of functionally active and stable protein conformations. Subsequent molecular docking analysis revealed the potential binding affinity of the proteins towards meta-eugenol. The docking scores, represented as binding energies, detected favorable interactions, suggesting that the complexes are energetically stable (Table 2).

The stability and specificity of the docked complexes were supported by multiple non-covalent interactions. This included van der Waals forces, alkyl and π-alkyl interactions, as well as carbon-hydrogen bonding between the ligand and amino acid residues within the binding pocket (Table 2). Such interactions play crucial roles in stabilizing the ligand–receptor complex and are indicative of strong binding affinity and potential bioactivity of meta-eugenol against the target proteins.

The *in silico* study was conducted to provide molecular insights into the potential interaction between meta-eugenol and several target proteins through high-quality homology modeling and molecular docking approaches. Molecular docking results revealed that meta-eugenol binds with moderate to high affinity to all target proteins, with binding energies ranging from −4.7 to −6.3 kcal $mol^{-1}$. Among them, FabL displayed the highest binding affinity (−6.3 kcal $mol^{-1}$), indicating its potential as the most favorable meta-eugenol-binding candidate. This is particularly interesting given FabL's role in fatty acid biosynthesis, suggesting that meta-eugenol might act as a potential modulator of lipid metabolism in the target organism.

The molecular interactions were observed with the microbial proteins Afnor1, Afomt1, Afvbs1, 7AP3, and FabL. Specifically, the redox-regulating (Afnor1) and methyltransferase (Afomt1) activities were likely hindered, while enzymes involved in fatty acid synthesis (Afvbs1 and FabL) and ATP production (7AP3) show mildly disturbed functionality. As a result, essential cellular processes such as membrane biosynthesis, energy generation, and metabolic homeostasis are expected to proceed with moderate disruptions. Therefore, the antimicrobial effect of the oil affects direct enzymatic inhibition moderately, but in combination, nonspecific mechanisms such as membrane perturbation, oxidative stress induction, and alteration of cellular signaling pathways cumulatively impose physiological stress on the microorganism.

Open Access Article. Published on 01 2025. Downloaded on 21/06/2026 23:23:45.
This article is licensed under a Creative Commons Attribution-NonCommercial 3.0 Unported Licence.

The docking interactions were characterized by a combination of van der Waals forces, π–π stacking, alkyl/π-alkyl contacts, π-cation/π-sulfur interactions, and conventional hydrogen bonds, which are crucial for the stabilization of ligand–protein complexes. These interaction profiles are consistent with earlier reports demonstrating the biological activity of meta-eugenol as a membrane-disrupting agent and an inhibitor of microbial enzymes, which is largely attributed to its aromatic structure and hydrophobic properties. The observed binding patterns also support the hypothesis that meta-eugenol may exert its bioactivity through a multi-target mechanism, interacting with different enzymes or regulatory proteins within microbial cells.

## 4. Conclusion

The study illustrates the strong antimicrobial efficacy of an essential oil-based combination (SACEO) and its nanoencapsulated form, Ne-SACEO. The Ne-SACEO was characterized by FTIR, DLS, and zeta potential analysis and later examined for its efficacy against food-borne microbes. Ne-SACEO demonstrated noticeably lower MIC and MAIC values than its free equivalents, indicating a strong antifungal and antiaflatoxigenic effect against *A. flavus*. The nanoencapsulated oil also had a strong antioxidative effect. The antifungal effect of Ne-SACEO was confirmed by mechanistic experiments that showed substantial membrane disintegration, as evidenced by decreased ergosterol content, increased cation leakage, mitochondrial membrane potential (MMP) collapse, and release of 260/280 nm absorbing materials.

The broad-spectrum efficacy of Ne-SACEO was confirmed by antibacterial assessments against both Gram-positive (*B. cereus*) and Gram-negative (*E. coli*, *S. enterica*, and *S. flexneri*) pathogens, which revealed significantly decreased MIC values. The formulation caused membrane depolarisation, protein and nucleic acid leakage, and a rise in the membrane polarisation index, all of which contributed to the disintegration of the bacteria. By improving solubility, concealing volatile components, and stimulating specific bioactivity, the nanocarrier system offered an unambiguous benefit. The molecular docking study confirmed that meta-eugenol exhibits moderate to high binding affinity with key microbial target proteins, especially FabL, suggesting potential inhibition of fatty acid biosynthesis. Stabilizing non-covalent interactions supports strong ligand–receptor complexes. These findings verify the multi-target antimicrobial potential of meta-eugenol driven by its aromatic and hydrophobic properties.

Overall, the combination of *S. aromaticum* leaf and bud essential oils, especially in nanoencapsulated form, exhibits potent antibacterial, antifungal, and antiaflatoxigenic activity through a multi-targeted mechanism, establishing it as a promising natural biopreservative and therapeutic candidate for food and health applications. In the future, the long-term stability, cytotoxicity, and biocompatibility of the nanoformulation need further assessment and validation in food systems.

## Author contributions

Bhanu Prakash: conceptualization, supervision, funding acquisition, reviewing, project administration. Tanya Singh Raghuvanshi: experiments, resources, data collection, data curation, writing – original draft. Vishal Gupta: data collection.

## Conflicts of interest

The authors declare that they have no known competing financial interests or personal relationships that could have appeared to influence the work reported in this paper.

## Data availability

Data will be made available on request.

## Acknowledgements

We are grateful to the Institute of Eminence Scheme, Banaras Hindu University, Varanasi, India, for the financial support to our laboratory scheme no. R/Dev/D/IOE/Incentive/2021-22/32393 and Anusandhan National Research Foundation (ANRF), New Delhi, India (File No. ANRF/IRG/2024/000544/LS). Tanya Singh Raghuvanshi (CSIR-SRF) (File No. 09/0013(13320)/2022-EMR-I) is thankful to CSIR-New Delhi. The authors express gratitude to the CIL, the Department of Botany and the Department of Chemistry, Banaras Hindu University, Varanasi for DLS and FTIR analysis. Furthermore, the authors also acknowledge the Advanced Instrumentation and Research Facility (AIRF), JNU, New Delhi, for GC-MS analysis.

## References

1 T. Bintsis, Foodborne pathogens, *AIMS Microbiol.*, 2017, **3**, 529, DOI: 10.3934/microbiol.2017.3.529.
2 T. C. Bhalla, International laws and food-borne illness, in *Food Safety and Human Health*, Academic Press, 2019, pp. 319–371, DOI: 10.1016/B978-0-12-816333-7.00012-6.
3 S. Lei, S. Chen and Q. Zhong, Digital PCR for accurate quantification of pathogens: principles, applications, challenges and future prospects, *Int. J. Biol. Macromol.*, 2021, **184**, 750–759, DOI: 10.1016/j.ijbiomac.2021.06.132.
4 K. H. Byun, M. Kang, M. S. Koo, M. C. Lim, G. S. Ok and H. J. Kim, Potential risk of biofilm-forming *B. cereus* group in fresh-cut lettuce production chain, *Food Res. Int.*, 2024, **191**, 114692, DOI: 10.1016/j.foodres.2024.114692.
5 S. Brockett, M. K. Wolfe, A. Hamot, G. D. Appiah, E. D. Mintz and D. Lantagne, Associations among water, sanitation, and hygiene, and food exposures and typhoid fever in Case–Control studies: a systematic review and meta-analysis, *Am. J. Trop. Med. Hyg.*, 2020, **103**, 1020, DOI: 10.4269/ajtmh.19-0479.
6 M. B. Zaidi and T. Estrada-García, *Shigella*: a highly virulent and elusive pathogen, *Curr. Trop. Med. Rep.*, 2014, **1**, 81–87, DOI: 10.1007/s40475-014-0019-6.


© 2026 The Author(s). Published by the Royal Society of Chemistry

Open Access Article. Published on 01 2025. Downloaded on 21/06/2026 23:23:45. This article is licensed under a Creative Commons Attribution-NonCommercial 3.0 Unported Licence.

7 A. Gong, M. Song and J. Zhang, Current strategies in controlling *Aspergillus flavus* and aflatoxins in grains during storage: a review, *Sustainability*, 2024, **16**, 3171, DOI: 10.3390/su16083171.
8 S. Marchese, A. Polo, A. Ariano, S. Velotto, S. Costantini and L. Severino, Aflatoxin B1 and M1: Biological properties and their involvement in cancer development, *Toxins*, 2018, **10**, 214, DOI: 10.3390/toxins10060214.
9 A. Dhakal, M. F. Hashmi and E. Sbar, *Aflatoxin toxicity*, StatPearls, 2020.
10 T. M. Uddin, A. J. Chakraborty, A. Khusro, B. R. M. Zidan, S. Mitra, T. B. Emran and N. Koirala, Antibiotic resistance in microbes: history, mechanisms, therapeutic strategies and future prospects, *J. Infect. Public Health*, 2021, **14**, 1750–1766, DOI: 10.1016/j.jiph.2021.10.020.
11 H. Falleh, M. B. Jemaa, M. Saada and R. Ksouri, Essential oils: a promising eco-friendly food preservative, *Food Chem.*, 2020, **330**, 127268, DOI: 10.1016/j.foodchem.2020.127268.
12 V. K. Pandey, S. Srivastava, K. K. Dash, R. Singh, A. H. Dar, T. Singh and B. Kovacs, Bioactive properties of clove (*Syzygium aromaticum*) essential oil nanoemulsion: a comprehensive review, *Heliyon*, 2024, **10**, e240011, DOI: 10.1016/j.heliyon.2023.e22437.
13 C. B'Hymer, Residual solvent testing: a review of gas-chromatographic and alternative techniques, *Pharm. Res.*, 2003, **20**, 337–344, DOI: 10.1023/A:1022693516409.
14 S. Kiran and B. Prakash, Toxicity and biochemical efficacy of chemically characterized *Rosmarinus officinalis* essential oil against *Sitophilus oryzae* and *Oryzaephilus surinamensis*, *Ind. Crops Prod.*, 2015, **74**, 817–823, DOI: 10.1016/j.indcrop.2015.05.073.
15 A. Kumar, P. P. Singh and B. Prakash, Unravelling the antifungal and anti-aflatoxin B1 mechanism of chitosan nanocomposite incorporated with *Foeniculum vulgare* essential oil, *Carbohydr. Polym.*, 2020, **236**, 116050, DOI: 10.1016/j.carbpol.2020.116050.
16 H. E. Elsayed, E. M. El-Deeb, H. Taha, H. S. Taha, M. R. Elgindi and F. A. Moharram, Essential oils of *Psidium cattleianum* Sabine leaves and flowers: anti-inflammatory and cytotoxic activities, *Front. Chem.*, 2023, **11**, 1120432, DOI: 10.3389/fchem.2023.1120432.
17 M. S. Mady, H. E. Elsayed, N. F. Tawfik and F. A. Moharram, Volatiles extracted from *Melaleuca rugulosa* (Link) Craven leaves: comparative profiling, bioactivity screening, and metabolomic analysis, *BMC Complementary Med. Ther.*, 2024, **24**, 394, DOI: 10.1186/s12906-024-04683-z.
18 M. Safitri, N. Sulistyani, I. Wahyuningsih, D. Sylvia and A. Aprilliani, A comparative study of antibacterial, antioxidant activity and total content of phenolic compounds from a combination of clove and cinnamon essential oils, *Int. J. Appl. Pharm.*, 2024, **16**, 5, DOI: 10.22159/ijap.2024v16s5.52486.
19 M. Beyki, S. Zhaveh, S. T. Khalili, T. Rahmani-Cherati, A. Abollahi, M. Bayat and A. Mohsenifar, Encapsulation of *Mentha piperita* essential oils in chitosan–cinnamic acid nanogel with enhanced antimicrobial activity against *A. flavus*, *Ind. Crops Prod.*, 2014, **54**, 310–319, DOI: 10.1016/j.indcrop.2014.01.033.
20 M. M. Desouky, R. H. Abou-Saleh, T. A. Moussa and H. M. Fahmy, Nano-chitosan-coated, green-synthesized selenium nanoparticles as a novel antifungal agent against *Sclerotinia sclerotiorum*: *in vitro* study, *Sci. Rep.*, 2025, **15**, 1004, DOI: 10.1038/s41598-024-79574-x.
21 C. Socaciu, F. Fetea, F. Ranga, A. Bunea, F. Dulf, S. Socaci and A. Pintea, Attenuated total reflectance-Fourier transform infrared spectroscopy (ATR-FTIR) coupled with chemometrics, to control the botanical authenticity and quality of cold-pressed functional oils commercialized in Romania, *Appl. Sci.*, 2020, **10**, 8695, DOI: 10.3390/app10238695.
22 A. Kumar, T. S. Raghuvanshi, V. Gupta, Vivekanand, N. Kohar and B. Prakash, Investigating the efficacy of chitosan-enriched *Cuminum cyminum* essential oil against food-borne molds, aflatoxin B1, and post-harvest quality of *Arachis hypogaea* L, *Food Biophys.*, 2024, **19**, 982–993, DOI: 10.1007/s11483-024-09877-z.
23 S. F. Abbas, A. J. Haider and S. Al-Musawi, Antimicrobial and wound healing effects of metal oxide nanoparticles-enriched wound dressing, *Nano*, 2023, **18**(08), 2330005, DOI: 10.1142/S1793292023300050.
24 S. F. Abbas, A. J. Haider, S. Al-Musawi and M. K. Selman, Antibacterial effect of copper oxide nanoparticles prepared by laser production in water against staphylococcus aureus and *Escherichia Coli*, *Plasmonics*, 2024, **19**(5), 2401–2411, DOI: 10.1007/s11468-023-02135-x.
25 A. Onyebuchi and D. Kavaz, Chitosan and *N*,*N*,*N*-trimethyl chitosan nanoparticle encapsulation of *Ocimum gratissimum* essential oil: Optimised synthesis, *in vitro* release and bioactivity, *Int. J. Nanomed.*, 2019, **14**, 7707–7727, DOI: 10.2147/IJN.S220202.
26 S. F. Hosseini, M. Zandi, M. Rezaei and F. Farahmandghavi, Two-step method for encapsulation of oregano essential oil in chitosan nanoparticles: preparation, characterization and *in vitro* release study, *Carbohydr. Polym.*, 2013, **95**(1), 50–56, DOI: 10.1016/j.carbpol.2013.02.031.
27 M. Asprea, I. Leto, M. C. Bergonzi and A. R. Bilia, Thyme essential oil loaded in nanocochleates: encapsulation efficiency, *in vitro* release study and antioxidant activity, *LWT–Food Sci. Technol.*, 2017, **77**, 497–502, DOI: 10.1016/j.lwt.2016.12.006.
28 S. Insawang, P. Pripdeevech, C. Tanapichatsakul, S. Khruengsai, S. Monggoot, T. Nakham and P. Panuwet, Essential oil compositions and antibacterial and antioxidant activities of five *Lavandula stoechas* cultivars grown in Thailand, *Chem. Biodiversity*, 2019, **16**, e1900371, DOI: 10.1002/cbdv.201900371.
29 T. Sripahco, S. Khruengsai, R. Charoensup, J. Tovaranonte and P. Pripdeevech, Chemical composition, antioxidant, and antimicrobial activity of *Elsholtzia beddomei* CB Clarke ex Hook. f. essential oil, *Sci. Rep.*, 2022, **12**, 2225, DOI: 10.1038/s41598-022-06358-6.
30 B. Prakash, R. Shukla, P. Singh, P. K. Mishra, N. K. Dubey and R. N. Kharwar, Efficacy of chemically characterized

Open Access Article. Published on 01 2025. Downloaded on 21/06/2026 23:23:45. This article is licensed under a Creative Commons Attribution-NonCommercial 3.0 Unported Licence.

*Ocimum gratissimum* L. essential oil as an antioxidant and a safe plant based antimicrobial against fungal and aflatoxin B1 contamination of spices, *Food Res. Int.*, 2011, **44**, 385–390, DOI: 10.1016/j.foodres.2010.10.002.

31 A. K. Pandey, N. Sonker and P. Singh, Efficacy of some essential oils against *Aspergillus flavus* with special reference to *Lippia alba* oil: an inhibitor of fungal proliferation and aflatoxin B1 production in green gram seeds during storage, *J. Food Sci.*, 2016, **81**, M928–M934, DOI: 10.1111/1750-3841.13254.

32 P. P. Singh, A. K. Jaiswal, T. S. Raghuvanshi and B. Prakash, Insights into the antimicrobial efficacy of *Coleus aromaticus* essential oil against food-borne microbes: biochemical and molecular simulation approaches, *Food Chem. Toxicol.*, 2023, **182**, 114111, DOI: 10.1016/j.fct.2023.114111.

33 A. Belasli, Y. Ben Miri, M. Aboudaou, L. Aït Ouahioune, L. Montañes, A. Ariño and D. Djenane, Antifungal, antitoxigenic, and antioxidant activities of the essential oil from laurel (*Laurus nobilis* L.): potential use as wheat preservative, *Food Sci. Nutr.*, 2020, **8**, 4717–4729, DOI: 10.1002/fsn3.1650.

34 A. Ma, X. Ban, B. Huang, J. He, J. Tian, H. Zeng and Y. Wang, Interference and mechanism of dill seed essential oil and contribution of carvone and limonene in preventing sclerotinia rot of rapeseed, *PLoS One*, 2015, **10**, e0131733, DOI: 10.1371/journal.pone.0131733.

35 F. Xiang, Q. Zhao, K. Zhao, H. Pei and F. Tao, The efficacy of composite essential oils against aflatoxigenic fungus *Aspergillus flavus* in maize, *Toxins*, 2020, **12**, 562, DOI: 10.3390/toxins12090562.

36 J. Tian, X. Ban, H. Zeng, J. He, Y. Chen and Y. Wang, The mechanism of antifungal action of essential oil from dill (*Anethum graveolens* L.) on *Aspergillus flavus*, *PLoS One*, 2012, **7**, e30147, DOI: 10.1371/journal.pone.0030147.

37 C. Song, W. Shi, J. Yang, G. Ding, W. Chen, C. Jia and J. Qin, Mechanism study on Monarda didyma essential oil inhibiting Aspergillus flavus infection and aflatoxins accumulation in peanuts, *Ind. Crops Prod.*, 2024, **212**, 118311, DOI: 10.1016/j.indcrop.2024.118311.

38 J. M. Fuentes, I. Jofré, G. Tortella, A. Benavides-Mendoza, M. C. Diez, O. Rubilar and P. Fincheira, The mechanistic insights of essential oil of Mentha piperita to control Botrytis cinerea and the prospection of lipid nanoparticles to its application, *Microbiol. Res.*, 2024, **286**, 127792, DOI: 10.1016/j.micres.2024.127792.

39 H. Ye, S. Shen, J. Xu, S. Lin, Y. Yuan and G. S. Jones, Synergistic interactions of cinnamaldehyde in combination with carvacrol against food-borne bacteria, *Food Control*, 2013, **34**, 619–623, DOI: 10.1016/j.foodcont.2013.05.032.

40 R. Requena, M. Vargas and A. Chiralt, Study of the potential synergistic antibacterial activity of essential oil components using the thiazolyl blue tetrazolium bromide (MTT) assay, *LWT–Food Sci. Technol.*, 2019, **101**, 183–190, DOI: 10.1016/j.lwt.2018.10.093.

41 Q. He, L. Zhang, Z. Yang, T. Ding, X. Ye, D. Liu and M. Guo, Antibacterial mechanisms of thyme essential oil nanoemulsions against *Escherichia coli* O157:H7 and *Staphylococcus aureus*: alterations in membrane compositions and characteristics, *Innov. Food Sci. Emerg. Technol.*, 2022, **75**, 102902, DOI: 10.1016/j.ifset.2021.102902.

42 Q. He, D. Liu, M. Ashokkumar, X. Ye, T. Z. Jin and M. Guo, Antibacterial mechanism of ultrasound against *Escherichia coli*: alterations in membrane microstructures and properties, *Ultrason. Sonochem.*, 2021, **73**, 105509, DOI: 10.1016/j.ultsonch.2021.105509.

43 W. de Souza Moura, S. R. de Souza, F. S. Campos, A. S. R. Cangussu, E. M. S. Santos, B. S. Andrade and R. W. de Souza Aguiar, Antibacterial activity of *Siparuna guianensis* essential oil mediated by impairment of membrane permeability and replication of pathogenic bacteria, *Ind. Crops Prod.*, 2020, **146**, 112142, DOI: 10.1016/j.indcrop.2020.112142.

44 J. Zhang, K. P. Ye, X. Zhang, D. D. Pan, Y. Y. Sun and J. X. Cao, Antibacterial activity and mechanism of action of black pepper essential oil on meat-borne *E. coli*, *Front. Microbiol.*, 2017, **7**, 2094, DOI: 10.3389/fmicb.2016.02094.

45 A. A. Heller and D. M. Spence, A rapid method for post-antibiotic bacterial susceptibility testing, *PLoS One*, 2019, **14**, e0210534, DOI: 10.1371/journal.pone.0210534.

46 S. Bienert, A. Waterhouse, T. A. de Beer, G. Tauriello, G. Studer, L. Bordoli and T. Schwede, The SWISS-MODEL Repository—new features and functionality, *Nucleic Acids Res.*, 2017, **45**, D313–D319, DOI: 10.1093/nar/gkw1132.

47 A. Waterhouse, M. Bertoni, S. Bienert, G. Studer, G. Tauriello, R. Gumienny, F. T. Heer, T. A. P. de Beer, C. Rempfer, L. Bordoli, R. Lepore and T. Schwede, SWISS-MODEL: homology modelling of protein structures and complexes, *Nucleic Acids Res.*, 2018, **46**, W296–W303, DOI: 10.1093/nar/gky427.

48 G. Studer, C. Rempfer, A. M. Waterhouse, R. Gumienny, J. Haas and T. Schwede, QMEANDisCo—distance constraints applied on model quality estimation, *Bioinformatics*, 2020, **36**, 1765–1771, DOI: 10.1093/bioinformatics/btz828.

49 A. Wlodawer, Stereochemistry and validation of macromolecular structures, in *Protein crystallography: methods and protocols*, 2017, pp. 595–610, DOI: 10.1007/978-1-4939-7000-1_24.

50 S. S. Butt, Y. Badshah, M. Shabbir and M. Rafiq, Molecular docking using chimera and autodock vina software for nonbioinformaticians, *JMIR Bioinf. Biotechnol.*, 2020, **1**(1), e14232, DOI: 10.2196/14232.

51 S. Y. B. de Carvalho, R. R. Almeida, N. A. R. Pinto, C. de Mayrinck, S. S. Vieira, J. F. Haddad and L. G. D. L. Guimaraes, Encapsulation of essential oils using cinnamic acid grafted chitosan nanogel: Preparation, characterization and antifungal activity, *Int. J. Biol. Macromol.*, 2021, **166**, 902–912, DOI: 10.1016/j.ijbiomac.2020.10.247.

52 M. Soltanzadeh, S. H. Peighambardoust, B. Ghanbarzadeh, M. Mohammadi and J. M. Lorenzo, Chitosan nanoparticles encapsulating lemongrass (*Cymbopogon commutatus*) essential oil: Physicochemical, structural, antimicrobial


© 2026 The Author(s). Published by the Royal Society of Chemistry

Open Access Article. Published on 01 2025. Downloaded on 21/06/2026 23:23:45.
This article is licensed under a Creative Commons Attribution-NonCommercial 3.0 Unported Licence.

and *in vitro* release properties, *Int. J. Biol. Macromol.*, 2021, **192**, 1084–1097, DOI: 10.1016/j.ijbiomac.2021.10.070.

53 M. Yousefi, V. G. Mohammadi, M. Shadnoush, N. Khorshidian and A. M. Mortazavian, *Zingiber officinale* essential oil-loaded chitosan-tripolyphosphate nanoparticles: fabrication, characterization and *in vitro* antioxidant and antibacterial activities, *Food Sci. Technol. Int.*, 2022, **28**, 592–602, DOI: 10.1177/10820132211040917.

54 A. Gordillo-Galeano and C. E. Mora-Huertas, Hydrodynamic diameter and zeta potential of nanostructured lipid carriers: emphasizing some parameters for correct measurements, *Colloids Surf. A Physicochem. Eng. Asp.*, 2021, **620**, 126610, DOI: 10.1016/j.colsurfa.2021.126610.

55 V. Rajkumar, C. Gunasekaran, C. A. Paul and J. Dharmaraj, Development of encapsulated peppermint essential oil in chitosan nanoparticles: characterization and biological efficacy against stored-grain pest control, *Pestic. Biochem. Physiol.*, 2020, **170**, 104679, DOI: 10.1016/j.pestbp.2020.104679.

56 M. S. Culas, D. G. Popovich and A. Rashidinejad, Recent advances in encapsulation techniques for cinnamon bioactive compounds: a review on stability, effectiveness, and potential applications, *Food Biosci.*, 2024, **57**, 103470, DOI: 10.1016/j.fbio.2023.103470.

57 B. Prakash, P. Singh, P. K. Mishra and N. K. Dubey, Safety assessment of Zanthoxylum alatum Roxb. essential oil, its antifungal, antiaflatoxin, antioxidant activity and efficacy as antimicrobial in preservation of *Piper nigrum* L. fruits, *Int. J. Food Microbiol.*, 2012, **153**(1–2), 183–191, DOI: 10.1016/j.ijfoodmicro.2011.11.007.

58 X. X. Lu, Y. Y. Zhu, F. Cheng, T. Wu and M. Maiwulanjiang, Ajwain essential oil inhibits aflatoxin B1 and ergosterol production in *Aspergillus flavus*: mechanisms and developmental stages-specific effects, *Food Biosci.*, 2024, **62**, 105561, DOI: 10.1016/j.fbio.2024.105561.

59 S. Tiwari, N. Upadhyay, B. K. Singh, V. K. Singh and N. K. Dubey, Chemically characterized nanoencapsulated *Homalomena aromatica* Schott. essential oil as green preservative against fungal and aflatoxin B1 contamination of stored spices based on *in vitro* and *in situ* efficacy and favorable safety profile on mice, *Environ. Sci. Pollut. Res.*, 2022, **29**, 3091–3106, DOI: 10.1007/s11356-021-15794-2.

60 M. Sindhu, V. Rajkumar, C. A. Annapoorani, C. Gunasekaran and M. Kannan, Nanoencapsulation of garlic essential oil using chitosan nanopolymer and its antifungal and anti-aflatoxin B1 efficacy *in vitro* and *in situ*, *Int. J. Biol. Macromol.*, 2023, **243**, 125160, DOI: 10.1016/j.ijbiomac.2023.125160.

61 D. Zhao, Y. Ma, W. Wang and Q. Xiang, Antibacterial activity and mechanism of cinnamon essential oil nanoemulsion against *Pseudomonas deceptionensis* CM2, *Heliyon*, 2023, **9**, e19543, DOI: 10.1016/j.heliyon.2023.e19543.

62 W. K. Costa, A. M. de Oliveira, I. B. da Silva Santos, V. B. G. Silva, E. K. C. da Silva, J. V. de Oliveira Alves and M. V. da Silva, Antibacterial mechanism of *Eugenia stipitata* McVaugh essential oil and synergistic effect against *Staphylococcus aureus*, *S. Afr. J. Bot.*, 2022, **147**, 724–730, DOI: 10.1016/j.sajb.2022.03.012.